Deciphering the genetic interactions between Pou4f3, Gfi1 and Rbm24 in maintaining cochlear hair cell survival

Guangqin Wang[1,2], Yunpeng Gu[1,2], Zhiyong Liu[1,2,3*]

1. Institute of Neuroscience, State Key Laboratory of Neuroscience, CAS Center for Excellence in Brain Science and Intelligence Technology, Chinese Academy of Sciences, Shanghai, 200031, China
2. University of Chinese Academy of Sciences, Beijing, 100049, China
3. Shanghai Center for Brain Science and Brain-Inspired Intelligence Technology, Shanghai, 201210, China

* Corresponding authors:
Dr. Zhiyong Liu; E-mail: Zhiyongliu@ion.ac.cn
Tel: 0086-21-54921793 (Office)

Key words: Pou4f3, Gfi1, Rbm24, hair cells, cochlea

ABSTRACT

Mammals have limited sound receptor hair cells (HCs) that cannot be regenerated after damage. Thus, investigating the molecular mechanisms underlying how to maintain HC survival is crucial to prevent hearing impairment. The *Pou4f3*$^{-/-}$ or *Gfi1*$^{-/-}$ HCs initially form but rapidly degenerate, whereas *Rbm24*$^{-/-}$ HCs degenerate much later. It remains elusive about the transcriptional cascades among Pou4f3, Gfi1 and Rbm24. Here, we demonstrate that *Rbm24* expression is completely repressed in *Pou4f3*$^{-/-}$ HCs, but its expression is not altered in *Gfi1*$^{-/-}$ HCs. Moreover, both Pou4f3 and Gfi1 expressions are intact in *Rbm24*$^{-/-}$ HCs. Moreover, by the *in vivo* mouse transgenic reporter assays, we identify three *Rbm24* enhancers to which Pou4f3 binds. Finally, we test whether Rbm24 restoration can alleviate degeneration of *Pou4f3*$^{-/-}$ HCs. Our *in vivo* genetic assay shows that ectopic Rbm24 alone is unable to stop *Pou4f3*$^{-/-}$ HCs from undergoing degeneration. Collectively, our study provides new molecular and genetic insights into how HC survival is regulated.

INTRODUCTION

Housed in the mammalian cochlea, the auditory epithelium, also referred to as the Organ of Corti (OC), contains the mechanosensory receptors hair cells (HCs) that detect sound information [1,2]. Two types of HCs exist: inner HCs (IHCs) and outer HCs (OHCs), with one row of IHCs and three rows of OHCs [3]. OHCs and IHCs derive from the cochlear progenitors experiencing high level of Atoh1, a master transcription factor (TF) in HC development [4-6]. No HCs are formed in *Atoh1* $^{-/-}$ cochleae, highlighting the essential roles of Atoh1 in specifying the general HC fates in the undifferentiated progenitors [7,8]. OHCs uniquely express motor protein Prestin (encoded by *Slc26a5*) and serve as sound amplifiers [9,10]. In contrast, IHCs specifically express Fgf8, vGlut3 (encoded by *Slc17a8*) and Otoferlin [11-15], acting as the primary sensory cells that form synapses with different subtypes of type I spiral (auditory) neurons [16-19]. Insm1 is necessary in stabilizing OHC fate, and ~50% of *Insm1*$^{-/-}$ OHCs tend to transdifferentiate into IHC-like cells [20,21]. Ikzf2 is not needed in early OHC development but is required in consolidating the OHC fate, and *Ikzf2* $^{cello/cello}$ deficient OHCs are dysfunctional and misexpress IHC genes [22]. Insm1 is an epistatic but indirect positive regulator of Ikzf2, and restoration of Ikzf2 can partially mitigate the phenotypes of *Insm1*$^{-/-}$ OHCs [21]. In contrast to Insm1 and Ikzf2, Tbx2 is required in IHC fate specification, differentiation, and maintenance, and IHC to OHC conversion occurs in the absence of Tbx2 [23-25].

It is necessary to maintain the survival of cochlear HCs after their production. Pou4f3, a POU-domain family TF and known hearing loss gene (DFNA15), is essential for HCs to survive [26-30]. Different from Atoh1, Pou4f3 is not involved in fate determination of HCs [31]. As one target gene regulated by Atoh1 [27,32], *Pou4f3* is turned on in HCs between E14.5 and E16 in

a basal to apical gradient, and subsequently Pou4f3 activates *Gfi1,* another zinc finger TF [33,34]. Gfi1 becomes undetectable in *Pou4f3*-deficient HCs [34]. HCs, especially the OHCs, degenerate in *Pou4f3* and *Gfi1*- mutants by birth [34]. Besides Pou4f3 and Gfi1, RNA binding protein Rbm24 is also specifically expressed in cochlear HCs [35]. Our recent study shows that Rbm24 is indispensable in maintaining the survival of OHCs, but the OHC death happens much later than the case in *Pou4f3* and *Gfi1*-mutants, with OHCs develop normally by birth but the majority of them undergo cell death by postnatal day 19 (P19) in *Rbm24*$^{-/-}$ mice [36]. It remains elusive about how *Rbm24* is regulated during cochlear HC development.

The similar but delayed phenotype of OHC death in *Rbm24* mutants relative to *Pou4f3* and *Gfi1*-deficient mice prompted us to dissect the potential genetic interactions among them by utilizing *in vivo* genetic approach. Our data clearly showed that onset of Rbm24 expression was completely repressed in *Pou4f3*$^{-/-}$ HCs. Surprisingly, Rbm24 expression was normal in *Gfi1*$^{-/-}$ HCs. Moreover, neither Pou4f3 nor Gfi1 expression was altered in the *Rbm24*$^{-/-}$ HCs. Thus, our data showed that Pou4f3, but not Gfi1, is required in *Rbm24* expression. Furthermore, we identified three *Rbm24* enhancers that were sufficient to drive specific EGFP reporter expression in HCs, which are likely bound by Pou4f3. Finally, restoration of Rbm24 alone cannot alleviate the degeneration of *Pou4f3*$^{-/-}$ HCs, highlighting that additional targeted genes of Pou4f3 are needed to be restored before keeping *Pou4f4*$^{-/-}$ HCs able to survive. In sum, our study provides new insights into the genetic interactions among Pou4f3, Gfi1 and Rbm24, with potential applications into HC protection.

RESULTS

Rbm24 expression is completely repressed in *Pou4f3* $^{-/-}$ cochlear HCs

HC degeneration happens in both *Pou4f3*$^{-/-}$ and *Rbm24*$^{-/-}$ mice, with the phenotypes occur earlier and are more severe in *Pou4f3*$^{-/-}$ mice [34,36]. It prompted us to speculate that genetic interaction between *Pou4f3* and *Rbm24* exists. Given Pou4f3 is the upstream positive regulator of Rbm24, Rbm24 expression should be blocked in the absence of Pou4f3. To rapidly determine whether it is the case, we took advantage of our previously established CRISPR-stop approach [37]. As illustrated in Supplemental Figure 1A, co-injecting one sgRNA-1 against *Pou4f3* and base editor components in one-cell stage mouse zygotes yielded founder 0 (F0) mice whose tail DNA was subjected to sanger sequencing. Relative to wild type (WT) mice (Supplemental Figure 1B), the F0 mice carrying the homozygous premature emergence of stop codon (TAG) were defined as *Pou4f3*$^{-/-}$ mice that were immediately ready for phenotypic analysis (Supplemental Figure 1C).

Triple staining of Pou4f3, Rbm24 and Insm1 demonstrated that OHCs were Pou4f3+/Rbm24+/Insm1+, and IHCs expressed Pou4f3 and Rbm24, but not Insm1 in basal turn of WT mice at E16.5 (n=3, Supplemental Figure 1D-D'''). Pou4f3 expression was completely absent in the *Pou4f3* $^{-/-}$ mice (n=9, Supplemental Figure 1E-E'''), confirming that Pou4f3 translation was blocked. Different from WT mice, Rbm24 expression completely disappeared in the *Pou4f3* $^{-/-}$ mice at E16.5 (Supplemental Figure 1E-E'''). Notably, Insm1 expression seemed normal in *Pou4f3* $^{-/-}$ mice (arrows in Supplemental Figure 1E-E'''), although we noticed that the alignment of Insm1+ OHCs was not as regular as the WT OHCs (Supplemental Figure 1D-D'''). Moreover, the presence of Insm1+ OHCs in the *Pou4f3* $^{-/-}$ mice

ruled out the possibility that the absence of Rbm24 was due to a secondary effect of OHC death or delayed differentiation, and also agreed with previous report that initial HC differentiation can occur without Pou4f3 [31,34]. Thus, the rapid *Pou4f3* loss-of-function analysis by CRISPR-stop supports our hypothesis that Pou4f3 is required in turning on Rbm24 expression.

To further validate the observation above, we also constructed a germ line stable *Pou4f3* mutants in which the entire Pou4f3 genome between sgRNA-2 and sgRNA-3 was deleted (Figure 1A). The three genotypes of *Pou4f3*$^{+/+}$, *Pou4f3*$^{+/-}$ and *Pou4f3*$^{-/-}$ were readily distinguished by tail DNA PCR (Figure 1B). Relative to WT mice (n=3, Figure 1C), Rbm24 again was completely absent in *Pou4f3*$^{-/-}$ mice at E16.5 (n=3, Figure 1D). Like Insm1, Bcl11b is another OHC marker [20]. Triple staining of Rbm24, Pou4f3 and Bcl11b also demonstrated that, relative to WT HCs (Figure 1E-E'''), Rbm24 was completely absent in *Pou4f3*$^{-/-}$ HCs (Figure 1F-F'''). Presence of Bcl11b+ OHCs also confirmed that production of nascent OHCs were normal in the absence of Pou4f3. Moreover, in contrast to WT mice at P1 (n=3, Supplemental Figure 2A-A''), HC degeneration was manifest in the germ line *Pou4f3*$^{-/-}$ mutants at P0 (n=4, Supplemental Figure 2B-B'') and P1 (n=3, Supplemental Figure 2C-C''). By normalizing numbers of the remaining HCs in *Pou4f3*$^{-/-}$ mice at P0 or P1 to those in WT mice at P1, we found that in P0 *Pou4f3*$^{-/-}$ mice, 35.94% ± 4.52%, 38.16% ± 2.79% and 63.8% ± 5.28% HCs survived in basal, middle and apical turns, respectively. However, in P1 *Pou4f3*$^{-/-}$ mice, 5.54% ± 3.11%, 15.79% ± 3.65% and 65.64% ± 7.95% of the HCs respectively survived in basal, middle and apical turns. Thus, HC degeneration at middle and basal turns was more severe (** $p<0.01$) at P1 than that at P0, but there was no significant difference in apical turns (Supplemental Figure 2D).

Different from WT cochleae in which all Myo7a+ HCs expressed Rbm24 (Supplemental Figure 2E-E''), in *Pou4f3*$^{-/-}$ cochleae the remaining HCs lost Rbm24 expression (arrows in Supplemental Figure 2F-F''). Collectively, our data from two different *Pou4f3*-deficient models support that Pou4f3 is indispensable for turning on *Rbm24*. Nonetheless, whether Gfi1 is also essential for Rbm24 expression remains to be determined.

Construction of a *Gfi1-3×HA-P2A-Cre/+* knockin mouse strain

We determined whether the regulation of *Rbm24* by Pou4f3 through Gfi1 or independently of Gfi1. Due to lack of a good commercial Gfi1 antibody suitable for immunostaining, we decided to construct a *Gfi1-3×HA-P2A-Cre/+* (*Gfi1*$^{HA\text{-}Cre/+}$ in brief) knockin mouse strain via our routine CRISPR/Cas9 approach (Supplemental Figure 3A-C). In principle, the C-terminus of Gfi1 was tagged with three HA fragments, and the Cre is under the endogenous *cis*-regulatory elements of *Gfi1*. The WT (*Gfi1*$^{+/+}$), heterozygous (*Gfi1*$^{HA\text{-}Cre/+}$) and homozygous (*Gfi1*$^{HA\text{-}Cre/HA\text{-}Cre}$) mice were readily distinguished by tail PCR (Supplemental Figure 3D). In addition to the *Gfi1* locus, Southern blot assay showed that random insertion of the targeting vector (Supplemental Figure 3B) happened in the unknown genomic region. Nonetheless, it was likely that the random insertion happened in a silent genomic region, which was evidenced by the analysis below.

Dual staining of HA (Gfi1) and pan-HC marker Myo7a demonstrated that, similar to *Gfi1*$^{+/+}$ mice (n=3, Supplemental Figure 3E-E''), HC development in *Gfi1*$^{HA\text{-}Cre/HA\text{-}Cre}$ was normal at P1 (n=3, Supplemental Figure 3F-F''). Moreover, HA (Gfi1) was highly expressed in all Myo7a+ IHCs and OHCs in *Gfi1*$^{HA\text{-}Cre/HA\text{-}Cre}$ mice (arrows in Supplemental Figure 3F-F''). It confirmed that Gfi1 endogenous expression is not affected in the *Gfi1*$^{HA\text{-}Cre/HA\text{-}Cre}$ mice,

representing an advantage over the previous *Gfi1*$^{Cre/+}$ strain where one copy of *Gfi1* is lost and early onset of hearing loss happens in *Gfi1*$^{Cre/+}$ [38,39].

We additionally performed the fate mapping analysis of *Gfi1*$^{HA\text{-}Cre/+}$*; Rosa26-loxp-stop-loxp-tdTomato (*Ai9*)/+* (*Gfi1*$^{HA\text{-}Cre/+}$; Ai9/+) at P2. The *Gfi1*$^{HA\text{-}Cre/+}$*;* Ai9/+ model allowed us to both visualize temporal Gfi1 protein expression pattern and permanently mark cells experiencing *Gfi1* expression with tdTomato. Neither tdTomato nor HA was detected in the Myo7a+ HCs of the control Ai9/+ mice (n=5, Supplemental Figure 3G-G''' and I-I''). In contrast, majority of the Myo7a+ HCs expressed tdTomato and HA in the *Gfi1*$^{HA\text{-}Cre/+}$*;* Ai9/+ mice (n=5, Supplemental Figure 3H-H''' and J-J''). We noticed that the general HA (Gfi1) expression level in IHCs seemed higher than that in OHCs (Supplemental Figure 3J-J''). Moreover, HA (Gfi1) expression levels exhibited manifest heterogeneities among OHCs. The OHCs expressing the highest (#1), intermediate (#2) and lowest (#3) levels of HA (Gfi1) were respectively marked (arrows in Supplemental Figure 3J-J''). Notably, such a heterogenous Gfi1 expression in neonatal HCs was not observed in *Gfi1*$^{HA\text{-}Cre/HA\text{-}Cre}$ mice (Supplemental Figure 3F-F''), likely due to the higher level of HA tagged Gfi1 in *Gfi1*$^{HA\text{-}Cre/HA\text{-}Cre}$ than in *Gfi1*$^{HA\text{-}Cre/+}$ mice. Besides HCs, tdTomato+ cells were present in the non-sensory regions (arrows in Supplemental Figure 3H), consistent with the previous report [38]. Collectively, *Gfi1*$^{HA\text{-}Cre/+}$ strain was suitable to visualize Gfi1 protein by HA antibody, albeit random insertion of the targeting vector existed. Alternatively, *Gfi1*$^{HA\text{-}Cre/+}$ at least can be treated as a pseudo transgenic mouse strain, by which we can reliably visualize Gfi1 and trace cells experiencing *Gfi1* expression.

Gfi1 expression is prohibited in the *Pou4f3*$^{-/-}$ cochlear HCs

Given HA can faithfully represent the Gfi1 expression in the *Gfi1*$^{HA\text{-}Cre/+}$, HA expression

was expected to be repressed in the *Pou4f3*$^{-/-}$ HCs, as reported by previous studies [33,34]. We confirmed this predication by our CRISPR-stop approach [37]. Basically, the pipeline was identical to the production of *Pou4f3* mutants described above (Supplemental Figure 1), except that here the zygotes were derived from male *Gfi1*$^{HA\text{-}Cre/+}$ mice (Supplemental Figure 4A). We obtained the mosaic (or chimeric) *Pou4f3*$^{-/-}$ mice, which was confirmed by Sanger sequencing of tail PCR (Supplemental Figure 4B and C), partly due to the injection time was the late stage of one-cell stage zygotes. In control *Gfi1*$^{HA\text{-}Cre/+}$ mice, there was a pure 'C' base (blue arrow in Supplemental Figure 4B), however, a mixture of 'C' and 'T' double peaks existed in *Gfi1*$^{HA\text{-}Cre/+}$; *Pou4f3*$^{-/-}$ (mosaic) mice (red arrow in Supplemental Figure 4C). Nonetheless, the advantage of the mosaic *Pou4f3*$^{-/-}$ mice was that it allowed us to have internal control *Pou4f3*$^{+/+}$ and *Pou4f3*$^{-/-}$ HCs in the same cochlea, and to determine the phenotype occurs in a cell autonomous or non-cell autonomous manner.

In control *Gfi1*$^{HA\text{-}Cre/+}$ mice (n=3) at E16.5, all HCs expressed Pou4f3, Rbm24 and HA(Gfi1), albeit HA (Gfi1) levels again seemed heterogenous among the OHCs (Supplemental Figure 4D-D'''). In contrast, in the *Gfi1*$^{HA\text{-}Cre/+}$; *Pou4f3*$^{-/-}$ (mosaic) mice (n=3), we captured HCs that lost or maintained Pou4f3 expression (Supplemental Figure 4E-E'''). Notably, Pou4f3+ HCs expressed HA(Gfi1) and Rbm24 (blue arrows in Supplemental Figure 4E-E'''), in contrast, both HA(Gfi1) and Rbm24 disappeared in HCs that lost Pou4f3 expression (orange arrows in Supplemental Figure 4E-E'''). Thus, our data clearly confirmed that HA indeed was a reliable readout for Gfi1 expression and was sensitive to loss of Pou4f3. Moreover, it supported that Pou4f3 regulates *Rbm24* in a cell autonomous manner.

Gfi1 is dispensable for Rbm24 expression

Next, we produced *Gfi1*$^{-/-}$ mutants by the same CRISPR-stop approach [37]. One-cell stage zygotes derived from male *Gfi1*$^{HA\text{-}Cre/+}$ mice were injected with base editor components and 4 different sgRNAs located in different exons of *Gfi1* (Figure 2A). The reason why 4 sgRNAs were combined was elaborated in the discussion part. With sgRNA-6 as an example, Sanger sequencing of tail DNA demonstrated that, relative to control *Gfi1*$^{HA\text{-}Cre/+}$ mice (black arrow in Figure 2B), premature emergence of TAG stop codon happened in F0 mice, resulting in homozygous Gfi1 inactivation (red arrow in Figure 2C). All HCs expressed HA (Gfi1) and Rbm24 in control *Gfi1*$^{HA\text{-}Cre/+}$ mice (n=3, Figure 2D-D''). Notably, Rbm24 expression was maintained in the *Gfi1*$^{-/-}$ HCs that lost HA (Gfi1) at E16.5 (n=4, Figure 2E-E''). It suggested that Rbm24 expression is not dependent on Gfi1.

The advantage of the above *Gfi1*$^{-/-}$ model was rapid and direct confirming the absence of Gfi1 expression in the F0 mice. However, we cannot guarantee that all HCs completely lost Gfi1 expression at the single cell resolution via HA staining, because only one allele of Gfi1 was *Gfi1*$^{HA\text{-}Cre}$. Thus, to rule out the possibility that only the HA tagged Gfi1 allele was mutated, we further generated the germ line stable *Gfi1* mutants in which its majority DNA fragments between sgRNA-4 and sgRNA-9 were deleted (Supplemental Figure 5A). The WT (*Gfi1*$^{+/+}$), *Gfi1*$^{+/-}$ and *Gfi1*$^{-/-}$ mice were readily to be identified by tail PCR (Supplemental Figure 5B). Consistent with previous reports [40], dual staining of Rbm24 and Pou4f3 showed that, relative to WT mice (n=3, Supplemental Figure 5C-C''), severe degeneration of HCs, especially of the OHCs, was present in the *Gfi1*$^{-/-}$ mice (n=3, Supplemental Figure 5D-D''). It validated the success of generating the *Gfi1*$^{-/-}$ mice. Notably, the surviving Pou4f3+ HCs kept the expression of Rbm24 (orange arrows in Supplemental Figure 5D-D''). In contrast, no significant

difference was observed between WT and *Gfi1*$^{-/-}$ mice at E16.5, as both WT and *Gfi1*$^{-/-}$ HCs expressed Pou4f3 and Rbm24, and both WT and *Gfi1*$^{-/-}$ OHCs expressed Bcl11b (Supplemental Figure 5E-F'''). It suggests that degeneration of *Gfi1*$^{-/-}$ HCs does not begin by E16.5. Presence of Pou4f3 in *Gfi1*$^{-/-}$ HCs agreed with previous notion that Pou4f3 is epistatic to Gfi1. Collectively, analysis of both *Gfi1* mutant models supports that Gfi1 is dispensable for Rbm24 expression.

Pou4f3 and Gfi1 expressions are normal in *Rbm24*$^{-/-}$ cochlear HCs

Given that Pou4f3 is upstream and positive regulator of *Rbm24*, we predicted that Pou4f3 expression should be unaffected in the *Rbm24*$^{-/-}$ HCs. To determine whether the predication was correct or not, we established the *Rbm24*$^{-/-}$ mouse strain by injecting one *Rbm24* sgRNA (sgRNA-10) into one-cell stage zygotes derived from male *Gfi1*$^{HA\text{-}Cre/+}$ mice (Figure 3A). We chose *Gfi1*$^{HA\text{-}Cre/+}$ zygotes in order to simultaneously assess Gfi1 and Pou4f3 expression patterns in *Rbm24*$^{-/-}$ HCs. Relative to the control *Gfi1*$^{HA\text{-}Cre/+}$; *Rbm24*$^{+/+}$ (Figure 3B), premature emerge of the TAG stop codon appeared in the *Gfi1*$^{HA\text{-}Cre/+}$; *Rbm24*$^{-/-}$ (mosaic) mice (Figure 3C). Notably, Sanger sequencing of tail DNA showed that the Rbm24 mutation was mosaic, as mixed 'T' and 'C' peak existed (red arrow in Figure 3C).

The mosaic inactivation of Rbm24 was further confirmed by triple staining of Rbm24, HA and Pou4f3 (Figure 3D-E'''). Relative to control *Gfi1*$^{HA\text{-}Cre/+}$; *Rbm24*$^{+/+}$ (n=3, Figure 3D-D'''), Rbm24 expression disappeared in a fraction of cochlear HCs (orange arrows in Figure 3E-E''') but remained normal in other HCs (blue arrows in Figure 3E-E''') of the *Gfi1*$^{HA\text{-}Cre/+}$; *Rbm24*$^{-/-}$ (mosaic) mice (n=3) at E17. Notably, regardless of whether Rbm24 was inactivated or not in the cochlear HCs, both HA (Gfi1) and Pou4f3 expression patterns were intact. It supports that

Pou4f3 is epistatic to Rbm24 and deletion of Rbm24 does not affect Pou4f3 expression. Moreover, our data suggests that Gfi1 and Rbm24 do not have genetic interactions. Gfi1 inactivation did not affect Rbm24 (Figure 2 and Supplemental Figure 5), and vice versa (Figure 3E-E''').

Three *Rbm24* enhancers can drive specific EGFP expression in cochlear HCs

After showing that Pou4f3, but not Gfi1, is indispensable in mediating *Rbm24* expression, we next determined the mechanism underlying how Pou4f3 controls *Rbm24* expression, in particular, the *cis*-regulation elements (CREs) of *Rbm24*. According to our previous Transposase-Accessible Chromatin with high-throughput sequencing (ATAC-seq) of neonatal cochlear HCs [8], four CREs of *Rbm24* were identified: one proximal promoter (arrow in Figure 4A) and three distal ones that were potential enhancers and defined as Eh1, Eh2 and Eh3, respectively (dotted square in Figure 4A). Eh1 and Eh2 were distributed upstream, whereas Eh3 was downstream of *Rbm24* coding region. Moreover, we reanalyzed the Pou4f3 Cut&Run assay from one previous study [32], and found that Pou4f3 binds to Eh1, Eh2 and Eh3, but not to the *Rbm24* promoter (Figure 4A).

Whether Eh1, Eh2 and Eh3 are bona-fide *Rbm24* enhancers remain to be determined. We reasoned that, if Eh1, Eh2 and Eh3 were *Rbm24* enhancers, either of them, together with the mini promoter of mouse heat shock protein 68 (Hsp68) [8,41-43], would be sufficient to drive specific reporter expression in cochlear HCs. To address this question, we established three transgenic mouse strains: Eh1-EGFP+ (n=7, Figure 4B-C''), Eh2-EGFP+ (n=6, Figure 4D-E'') and Eh3-EGFP+ (n=4, Figure 4F-G''). Briefly, in each strain the EGFP expression was driven by the mini promoter of Hsp68 and Eh1 (or Eh2 or Eh3). It is known that the mini promoter of

Hsp68 alone is not able to drive EGFP expression [44]. In contrast, strong EGFP expression was observed by whole mount analysis in all three transgenic lines (Figure 4B, D and F). Moreover, dual staining of EGFP and Myo7a in cryosectioned cochleae showed that EGFP was specifically expressed in IHCs and OHCs in all three strains at P1 (Figure 4C-C'', E-E'' and G-G''). Collectively, our transgenic assay supports that Eh1, Eh2 and Eh3 are *Rbm24* enhancers. Moreover, Pou4f3 mediates the *Rbm24* expression primarily by binding to *Rbm24* enhancers.

Forced Rbm24 expression fails to alleviate the degeneration of *Pou4f3*$^{-/-}$ HCs

Whether ectopic Rbm24 expression can alleviate the degeneration of *Pou4f3*$^{-/-}$ HCs remains unknown, albeit we showed that Rbm24 is certainly regulated by Pou4f3. Thus, we established a new conditional *Rosa26*-Loxp-stop-Loxp-Rbm24*3xHA/+ (*Rosa26*$^{Rbm24/+}$ in short) mouse model (Figure 5A and B). To turn on ectopic Rbm24 in cochlear HCs, *Rosa26*$^{Rbm24/+}$ was further crossed with the *Atoh1*$^{Cre/+}$ that targets majority of cochlear HCs and a fraction of SCs [39]. Notably, in the *Rosa26*$^{Rbm24/+}$ strain, Rbm24 was tagged with three HA fragments, which facilitated us to distinguish the endogenous and the ectopic Rbm24. In the control *Pou4f3*$^{+/+}$ (Figure 5C-C'') and the germ line stable *Pou4f3*$^{-/-}$ (Figure 5D-D'') mice, the Myo7a+ HCs did not express HA (Rbm24), however, almost of all Myo7a+ HCs expressed HA (Rbm24) in the *Pou4f3*$^{+/+}$; *Atoh1*$^{Cre/+}$; *Rosa26*$^{Rbm24/+}$ mice at P1 (white arrows in Figure 5E-E''). As expected, besides HCs, we captured a few SCs expressing HA (Rbm24) but not Myo7a (orange arrows in Figure 5E-E''). Those cochlear HCs expressing HA (Rbm24) seemed normal, suggesting that they can tolerate extra Rbm24 expression by P1. Collectively, it supports that the *Rosa26*$^{Rbm24/+}$ model was successfully generated and ectopic Rbm24 was induced in cochlear HCs in *Pou4f3*$^{+/+}$; *Atoh1*$^{Cre/+}$; *Rosa26*$^{Rbm24/+}$.

In contrast to our expectation, ectopic Rbm24 expression failed to mitigate the degeneration of *Pou4f3*$^{-/-}$ HCs. Severe degeneration of HCs (both IHCs and OHCs) occurred in *Pou4f3*$^{-/-}$; *Atoh1*$^{Cre/+}$; *Rosa26*$^{Rbm24/+}$ (Figure 5F-F''), indistinguishable from the *Pou4f3*$^{-/-}$ mice (Figure 5D-D''), except that the remaining HCs expressed Rbm24 in the *Pou4f3*$^{-/-}$; *Atoh1*$^{Cre/+}$; *Rosa26*$^{Rbm24/+}$ (arrows in Figure 5F-F''). It suggests that restoration of Rbm24 alone is not sufficient to prevent *Pou4f3*$^{-/-}$ cochlear HCs from undergoing degeneration.

DISCUSSION

Molecular mechanisms underlying cochlear HC survival

Our sound receptor HCs are vulnerable to various genetic mutations, environmental ototoxic factors and ageing. The degeneration of HCs is one of the primary reasons accounting for human sensorineural hearing impairment [45]. Previous studies have revealed many genes whose mutations lead to HC degeneration starting at different ages. Severe HC developmental defect happens in *Atoh1* $^{-/-}$ mutants [7,46]. It is known that *Atoh1*$^{-/-}$ cochlear sensory cells undergo apoptosis. Whether the absence of HCs in *Atoh1*$^{-/-}$ mice is due to that HCs are never produced, or immediately die after initial emergence remains unclear, partly due to the difficulty of unambiguously defining the nascent HCs by molecular markers.

Differently from *Atoh1*$^{-/-}$ mutants, in both *Pou4f3*$^{-/-}$ and *Gfi1*$^{-/-}$ mice [31,33,34], the initial cochlear HC development is normal but become defective at perinatal ages, consistent with the notion that Pou4f3 and Gfi1 are not required in HC fate specification but needed in subsequent differentiation and survival. It is known that caspase 3 is active during the hair cell death in the *Pou4f3*$^{-/-}$ mutants, and the anti-apoptotic factor z-VAD-fmk has a protective effect on the

Pou4f3$^{-/-}$ HCs between 14.5 and E16.5 [47]. Moreover, we noticed that the overall HC degeneration in *Gfi1*$^{-/-}$ was milder than in *Pou4f3*$^{-/-}$ mice at P1, because only OHC degeneration happened in the *Gfi1*$^{-/-}$, but both IHC and OHC were degenerated in *Pou4f3*$^{-/-}$ mice (Supplemental Figures 2 and 5).

It is known that *Gfi1* is the target of Pou4f3 [34]. Whether forced Gfi1 expression can alleviate the degeneration of *Pou4f3*$^{-/-}$ HCs remains unknown, too. Likewise, Pou4f3 is one of the target genes regulated by Atoh1 [32], however, whether forced expression of either Pou4f3 or Gfi1, or both Pou4f3 and Gfi1, is able to mitigate the developmental defects of *Atoh1*$^{-/-}$ HCs remains to be determined. Future studies are warranted to resolve those remaining questions before further deeply understanding the mechanisms underlying how to keep cochlear HCs to survive.

Roles of Rbm24 and how Rbm24 is regulated during cochlear HC development

Shortly after cochlear HCs emerge, Rbm24 is expressed and permanently maintained, evidenced by transcriptomic analyses and antibody staining [23,35,48-50]. Rbm24 is not necessary in early phase of cochlear HC development, because *Rbm24*$^{-/-}$ HC development is normal by P1, however, Rbm24 is required for OHC to survive after birth [36]. *Rbm24*$^{-/-}$ OHCs, but not IHCs, are degenerated by P19 [36]. Rbm24 is also involved in mRNA stability and pre-mRNA alternative splicing of genes including *Cdh23* and *Pcdh15* that are crucial for HC stereocilia development [51-53]. Nonetheless, the single-cell transcriptomic analysis of *Rbm24*$^{-/-}$ IHCs or OHCs is not yet available and the detailed molecular mechanism underlying *Rbm24*$^{-/-}$ HC degeneration remains to be clarified in future studies.

What are the *trans*-acting factors that are involved in regulating *Rbm24* expression? First,

our current study provided strong genetic evidence to support that Pou4f3 is needed in turning on *Rbm24*. In the absence of Pou4f3, Rbm24 expression cannot be triggered. The normal expression of Pou4f3 in *Rbm24*$^{-/-}$ HCs further confirmed that *Pou4f3* is epistatic to *Rbm24* and that Rbm24 is dispensable for *Pou4f3* expression. Besides Pou4f3, the engagement of Atoh1 in *Rbm24* regulation is supported by two lines of evidence: one is that *Rbm24* expression disappears in the *Atoh1*$^{-/-}$ cochlear HCs [54]; the second is that *Rbm24* belongs to the Atoh1 binding targets revealed by Atoh1 Cut&Run assay [8,32]. Notably, Atoh1 binds both *Rbm24* promoter and its three enhancers Eh1, Eh2 and Eh3 [8,32], which differs with Pou4f3 which only binds *Rbm24* enhancers (Figure 4). Thus, it is likely that Pou4f3 and Atoh1 cooperate to regulate *Rbm24*, and either *Pou4f3* or *Atoh1* mutation leads to repression of Rbm24 expression. Whether *Rbm24* expression in adult HCs needs Pou4f3 remains to be determined by future conditional *Pou4f3* loss-of-function studies.

Gfi1 and Rbm24 expression are independent to each other

We initially hypothesized that Pou4f3 mediated *Rbm24* expression through Gfi1. However, this hypothesis is not supported by the observation that Rbm24 expression is normal in the *Gfi1*$^{-/-}$ HCs (Figure 2 and Supplemental Figure 5). Moreover, in the absence of Rbm24, Gfi1 expression is not altered in cochlear HCs, either. Thus, Rbm24 and Gfi1 expressions seem independent to each other. It might be due to the functional difference between Pou4f3 and Gfi1 during cochlear HC development. Both Pou4f3 and Gfi1 are needed in promoting expression of genes involved in HC differentiation [28,30,34,40], however, Gfi1, but not Pou4f3, also represses the preceding neural genes expressed in nascent HCs [40].

Furthermore, we have another observation relevant to Gfi1 isoforms that is worthy of

discussion. Our previous report shows that one efficient sgRNA is enough to induce homozygous gene inactivation by CRISPR-stop [36]. Notably, we used 4 different *Gfi1* sgRNAs that are distributed in different exons (Figure 2A). We indeed successfully established one *Gfi1* mutant by using the sgRNA-5 alone which in principle would effectively pre-stop the Gfi1 translation in exon 1 coding SNAG repressor domain. This *Gfi1* mutant (sgRNA-5 alone) was able to yield the HC degeneration phenotype, but the HA (Gfi1) was still detectable in HCs. It is consistent with the notion that *Gfi1* mutant lacing the SNAG domain is equivalent to *Gfi1*-null model [55]. Thus, it is likely that Gfi1 has multiple unknown isoforms, many of which might be recognized by the HA tag antibody because HA is tagged in the last exon 6. When 4 *Gfi1* sgRNAs were combined, we were able to both reproduce the HC degeneration phenotype and completely block the HA (Gfi1) expression.

Why does ectopic Rbm24 fail to alleviate the degeneration of *Pou4f3*$^{-/-}$ HCs?

After confirming the epistatic genetic interaction between Pou4f3 and Rbm24, we predicted that ectopic Rbm24 expression should be able to, at least partly, alleviate the degeneration of *Pou4f3*$^{-/-}$ HCs, similar to the case between Insm1 and Ikzf2 in cochlear OHCs in our recent study [21]. However, the actual observation is that Rbm24 failed to rescue the HC degeneration in the *Pou4f3*$^{-/-}$ mice. There are two possible interpretations: 1) Despite it is regulated by Pou4f3, Rbm24 is not directly involved in the pathway regulating HC survival. Indeed, the cell death in *Rbm24*$^{-/-}$ HCs happens later than in *Pou4f3*$^{-/-}$ HCs; 2) Although *Rbm24* is a key Pou4f3 downstream target, its forced expression alone cannot compensate loss of Pou4f3 or other known Pou4f3 targets such as orphan thyroid nuclear receptor *Nr2f2* and *Caprin-1* [56,57]. *Caprin-1* is recruited to stress granules in cochlear HCs exposed to ototoxic

trauma [57].

The potential application of the three *Rbm24* enhancers in cochlear HC gene therapy

Gene therapy is a promising strategy to restore the hearing capacity in human inheriting gene mutations [45]. A few examples have been reported, including *Otoferlin* and *vGlut3* gene replacement [58-61]. Currently, the therapeutic cDNAs were primarily delivered into HCs with an adeno-associated virus (AAV) vector. Despite many AAVs are reported [62,63], their transfecting cochlear cells is non-selective and HC specific AAV is not available yet. One solution is that, instead of the CAG/CMV ubiquitous promoter widely used in current AAVs [64,65], either of the three *Rbm24* enhancers together with *Hsp68* mini promoter (in brief *Rbm24-Hsp68*) should be able to produce an AAV that would specifically transfect HCs. Moreover, *Rbm24* is permanently expressed in cochlear HCs. Given the *Rbm24-Hsp68* AAV works as expected, it would be a powerful tool for future HC specific gene therapy at all postnatal ages, with potential applications in treating clinical human deafness.

METHODS AND MATERIALS

Mice

The *Atoh1*$^{Cre/+}$ model was kindly provided by Dr Lin Gan (Augusta University, USA)[39]. The *Rosa26-loxp-stop-loxp-tdTomato (*Ai9*)/+* strain (Jax#: 007905) was from the Jackson Laboratory. All mice were bred and raised in a SPF-level animal room and all animal procedures were performed according to the guidelines (NA-032-2022) of the IACUC of the Institute of Neuroscience (ION), Center for Excellence in Brain Science and Intelligence Technology, Chinese Academy of Sciences.

One-step generation of homozygous *Pou4f3* or *Gfi1* or *Rbm24* mutants by CRISPR-stop

The detailed protocol of how to use CRISPR-stop to generate homozygous gene mutants is described in our previous report [36,37]. Briefly, efficient pre-tested sgRNAs (Table S1) and hA3ABE3 were co-injected into one-cell stage mouse zygotes that were subsequently transplanted into pseudopregnant female mice giving birth to the founder 0 (F0) mice. With Sanger sequencing of tail PCR, the F0 mice with homozygous mutation (pre-emergence of protein translation stop codon) were identified and immediately ready for analysis.

Generating *Pou4f3* or *Gfi1*-null mutants with large DNA fragment deletion by CRISPR/Cas9

To construct germ line stable null mutants of either *Pou4f3* or *Gfi1*, *Cas9* mRNA, two efficient pre-tested sgRNAs respectively located at the proximal and distal end of the targeted gene, together with a single strand DNA donor (120 bp) (Table S3), were co-injected into the one-cell stage wild type zygotes. Notably, the left half (60 bp) of the single strand DNA donor was homologous to the 5' end, and the right half (60 bp) was to the 3'end of the targeted gene. The post-injected zygotes were transplanted into pseudopregnant females that would give birth to the F0 mice subjected to tail PCR screening (primers were listed in Table S2). The F0 mice harboring the designed large DNA deletion between the two sgRNAs were identified and further bred with wild type mice to establish the germ-line stable mutants (F1 or afterward).

Construction of the *Gfi1*3 ×HA-P2A-Cre* knockin mouse strain

The sgRNA against *Gfi1* (5′-ATGGACTCAAATGAGTACCC-3′), *Cas9* mRNA and the targeting vector (Supplemental Figure 3B) were co-injected into the one-cell stage wild type mouse zygotes. The targeting vector contained three portions, 5' homologous arm (800 bp), 3'

homologous arm (800 bp) and the part in the middle of 5' and 3' arms that contained three HA fragments followed by 2A-Cre. The F0 mice with the potential gene targeting (Supplemental Figure 3C) were screened by tail PCR, followed by crossing with wild type mice to produce F1 mice. Those F1 mice were confirmed by tail PCR again, and further subjected to Southern blot. The detailed protocol of Southern blot is described in our previous report [66]. Tail DNA PCR was used for routine genotyping and primers used to distinguish between KI (*Gfi1*$^{HA\text{-}Cre/+}$) and WT alleles were F4, R5 and R6 (Table S2).

Construction of Eh1-EGFP+, Eh2-EGFP+ and Eh3-EGFP+ transgenic reporter lines

All three transgenic reporter mouse lines, Eh1-EGFP+, Eh2-EGFP+ and Eh3-EGFP+ were produced by the same experimental procedures. The core DNA sequences of each enhancer (Eh1 or Eh2 or Eh3 in Figure 4A), mRNA of PiggyBac transposase, and the PiggyBac vector (Figure 4B, D and F) were co-injected into the one-cell stage of wild type mouse zygotes. The PiggyBac vector contained Eh1/Eh2/Eh3 core DNA sequences (Table S3), mini promoter of mouse heat shock protein 68 (Hsp68) and the EGFP coding sequence. The PiggyBac vector was randomly integrated into mouse genome by the transposase. The F0 mice containing the PiggyBac vector were screened by tail PCR and further bred with wild type mice to produce germ line stable F1 transgenic reporter strains. The samples analyzed in Figure 4B-G'' were from F1 or afterwards. Primers used for genotyping transgenic reporter strain were F8, F9 and F10 and a common primer R11 and primer sequences were listed in Table S2.

Generation of *Rosa26*$^{CAG\text{-}lsl\text{-}Rbm24*3\times HA/+}$ mouse models

The *Rosa26*$^{CAG\text{-}lsl\text{-}Rbm24*3\times HA/+}$ (*Rosa26*$^{Rbm24/+}$) knockin mouse strain was constructed by homologous recombination mediated by CRISPR/Cas9. The pre-tested *Rosa26* sgRNA (5′-

ACTCCAGTCTTTCTAGAAGA-3′), targeting vector (Figure 5A), together with the mRNA of *Cas9* were co-injected into the one-cell stage wild type mouse zygotes. Similarly, F0 mice with potentially correct gene targeting were screened by tail PCR and further bred with wild type mice to establish germ line stable F1 mice. The primers used to distinguish wild type and the KI (*Rosa26*$^{Rbm24/+}$) alleles were F12, R13 and R14 (Table S2).

Sample processing and immunofluorescence assay

Inner ears were dissected and fixed in 4% paraformaldehyde (PFA) in PBS (E607016-0500, Sangon Biotech) at 4°C overnight. For cochlear cryosections, inner ears were dehydrated in 30% sucrose (V900116, Sigma) at 4°C before embedding into the optimal cutting temperature (OCT) compound (4583, SAKURA) and slices were cut with 14 μm thickness. The detailed protocol of immunofluorescent staining is described in our previous report [67]. The following primary antibodies were used: anti-Rbm24 (rabbit, 1:500, 18178-1-AP, Proteintech); anti-Pou4f3 (mouse, 1:500, sc-81980, Santa Cruz); anti-Pou4f3 (rabbit, 1:500, NBP1-88349, Novus Biologicals); anti-HA (rat, 1:500, 11867423001, Roche); anti-Myo7a (rabbit, 1:500, 25-6790, Proteus Biosciences); anti-Myo7a (mouse, 1:500, MYO7A 138-1, Developmental Studies Hybridoma Bank); anti-Ctip2 (Bcl11b) (rat, 1:500, ab18465, Abcam); anti-Insm1 (guinea pig, 1:6000, a kind gift from Dr. Carmen Birchmeier from Max Delbrueck Center for Molecular Medicine, Germany); anti-GFP (chicken, 1:500, ab13970, Abcam). Different corresponding Alexa Fluor-conjugated secondary antibodies were used for detecting the primary antibodies above. Hoechst 33342 (1:1000, H3570, Thermo Fisher Scientific) was used for nuclear DNA staining.

Lastly, either whole-mount or cryosection samples were mounted with Prolong Gold

antifade medium (P36930, Thermo Fisher Scientific) at room temperature for 12 h. Samples were scanned by the Nikon C2 or Nikon NiE-A1 Plus confocal microscope. ImageJ software was used to process the confocal images.

Cell quantification and statistical analysis

Before immunofluorescent staining, each cochlear sample was grossly separated into three portions but with different length. Each portion of the same cochlea was initially scanned with confocal microscope but at a low magnification (10 × lens). After calculating the total length of each cochlea, it was precisely divided into basal, middle and apical turn with equal length. Then, for cell counting in the experiments (Supplemental Figure 2D), in each turn ~200μm length of the sensory epithelium was scanned with confocal microscope but at a high magnification (60 × lens) by which the number of HCs was counted. In the *Pou4f3*$^{-/-}$ cochleae, the percentage of the surviving HCs was calculated by normalizing the number of the remaining HCs to the counterparts in the wild type mice. All cell numbers were presented as means ± SEM. For statistical analyses, we used GraphPad Prism 6.0 software and performed Student's *t* tests with Bonferroni correction.

REFERENCES:

1. Wu, D.K., and Kelley, M.W. (2012). Molecular mechanisms of inner ear development. Cold Spring Harb Perspect Biol *4*, a008409. 10.1101/cshperspect.a008409.

2. Qiu, X., and Muller, U. (2022). Sensing sound: Cellular specializations and molecular force sensors. Neuron *110*, 3667-3687. 10.1016/j.neuron.2022.09.018.

3. Groves, A.K., Zhang, K.D., and Fekete, D.M. (2013). The genetics of hair cell development and regeneration. Annu Rev Neurosci *36*, 361-381. 10.1146/annurev-neuro-062012-170309.

4. Li, S., Fan, T., Li, C., Wang, Y., Li, J., and Liu, Z. (2022). Fate-mapping analysis of cochlear cells expressing Atoh1 mRNA via a new Atoh1(3*HA-P2A-Cre) knockin mouse strain. Dev Dyn, DOI: 10.1002/dvdy.1453. 10.1002/dvdy.453.

5. Driver, E.C., Sillers, L., Coate, T.M., Rose, M.F., and Kelley, M.W. (2013). The Atoh1-lineage gives rise to hair cells and supporting cells within the mammalian cochlea. Dev Biol *376*, 86-98. 10.1016/j.ydbio.2013.01.005.

6. Matei, V., Pauley, S., Kaing, S., Rowitch, D., Beisel, K.W., Morris, K., Feng, F., Jones, K., Lee, J., and Fritzsch, B. (2005). Smaller inner ear sensory epithelia in Neurog 1 null mice are related to earlier hair cell cycle exit. Dev Dyn *234*, 633-650. 10.1002/dvdy.20551.

7. Bermingham, N.A., Hassan, B.A., Price, S.D., Vollrath, M.A., Ben-Arie, N., Eatock, R.A., Bellen, H.J., Lysakowski, A., and Zoghbi, H.Y. (1999). Math1: an essential gene for the generation of inner ear hair cells. Science *284*, 1837-1841.

8. Luo, Z., Du, Y., Li, S., Zhang, H., Shu, M., Zhang, D., He, S., Wang, G., Lu, F., and Liu, Z. (2022). Three distinct Atoh1 enhancers cooperate for sound receptor hair cell development. Proc Natl Acad Sci U S A *119*, e2119850119. 10.1073/pnas.2119850119.

9. Zheng, J., Shen, W., He, D.Z., Long, K.B., Madison, L.D., and Dallos, P. (2000). Prestin is the motor protein of cochlear outer hair cells. Nature *405*, 149-155. 10.1038/35012009.

10. Liberman, M.C., Gao, J., He, D.Z., Wu, X., Jia, S., and Zuo, J. (2002). Prestin is required for electromotility of the outer hair cell and for the cochlear amplifier. Nature *419*, 300-304. 10.1038/nature01059.

11. Ruel, J., Emery, S., Nouvian, R., Bersot, T., Amilhon, B., Van Rybroek, J.M., Rebillard, G., Lenoir, M., Eybalin, M., Delprat, B., et al. (2008). Impairment of SLC17A8 encoding vesicular glutamate transporter-3, VGLUT3, underlies nonsyndromic deafness DFNA25 and inner hair cell dysfunction in null mice. Am J Hum Genet *83*, 278-292. 10.1016/j.ajhg.2008.07.008.

12. Seal, R.P., Akil, O., Yi, E., Weber, C.M., Grant, L., Yoo, J., Clause, A., Kandler, K., Noebels, J.L., Glowatzki, E., et al. (2008). Sensorineural deafness and seizures in mice lacking vesicular glutamate transporter 3. Neuron *57*, 263-275. 10.1016/j.neuron.2007.11.032.

13. Roux, I., Safieddine, S., Nouvian, R., Grati, M., Simmler, M.C., Bahloul, A., Perfettini, I., Le Gall, M., Rostaing, P., Hamard, G., et al. (2006). Otoferlin, defective in a human deafness form, is essential for exocytosis at the auditory ribbon synapse. Cell *127*, 277-289. 10.1016/j.cell.2006.08.040.

14. Pan, Y., Li, S., He, S., Wang, G., Li, C., Liu, Z., and Xiang, M. (2023). Fgf8(P2A-3xGFP/+): A New Genetic Mouse Model for Specifically Labeling and Sorting Cochlear Inner Hair Cells. Neurosci Bull. 10.1007/s12264-023-01069-y.

15. Jacques, B.E., Montcouquiol, M.E., Layman, E.M., Lewandoski, M., and Kelley, M.W. (2007). Fgf8 induces pillar cell fate and regulates cellular patterning in the mammalian cochlea. Development *134*, 3021-3029. 10.1242/dev.02874.

16. Petitpre, C., Wu, H., Sharma, A., Tokarska, A., Fontanet, P., Wang, Y., Helmbacher, F., Yackle, K., Silberberg, G., Hadjab, S., and Lallemend, F. (2018). Neuronal heterogeneity and stereotyped connectivity in the auditory afferent system. Nat Commun *9*, 3691. 10.1038/s41467-018-06033-3.

17. Shrestha, B.R., Chia, C., Wu, L., Kujawa, S.G., Liberman, M.C., and Goodrich, L.V. (2018). Sensory Neuron Diversity in the Inner Ear Is Shaped by Activity. Cell *174*, 1229-1246 e1217. 10.1016/j.cell.2018.07.007.

18. Sun, S., Babola, T., Pregernig, G., So, K.S., Nguyen, M., Su, S.M., Palermo, A.T., Bergles, D.E., Burns, J.C., and Muller, U. (2018). Hair Cell Mechanotransduction Regulates Spontaneous Activity and Spiral Ganglion Subtype Specification in the Auditory System. Cell *174*, 1247-1263 e1215. 10.1016/j.cell.2018.07.008.

19. Zhang, D., Ren, M., Bi, Z., Gu, Y., Li, S., Wang, G., Li, X., and Liu, Z. (2023). Lypd1-DTR/+: A New Mouse Model for Specifically Damaging the Type Ic Spiral Ganglion Neurons of the Cochlea. Neurosci Bull. 10.1007/s12264-023-01071-4.

20. Wiwatpanit, T., Lorenzen, S.M., Cantu, J.A., Foo, C.Z., Hogan, A.K., Marquez, F., Clancy, J.C., Schipma, M.J., Cheatham, M.A., Duggan, A., and Garcia-Anoveros, J. (2018). Trans-differentiation of outer hair cells into inner hair cells in the absence of INSM1. Nature *563*, 691-695. 10.1038/s41586-018-0570-8.

21. Li, S., He, S., Lu, Y., Jia, S., and Liu, Z. (2023). Epistatic genetic interactions between Insm1 and Ikzf2 during cochlear outer hair cell development. Cell Rep *42*, 112504. 10.1016/j.celrep.2023.112504.

22. Chessum, L., Matern, M.S., Kelly, M.C., Johnson, S.L., Ogawa, Y., Milon, B., McMurray, M., Driver, E.C., Parker, A., Song, Y., et al. (2018). Helios is a key transcriptional regulator of outer hair cell maturation. Nature *563*, 696-700. 10.1038/s41586-018-0728-4.

23. Bi, Z., Li, X., Ren, M., Gu, Y., Zhu, T., Li, S., Wang, G., Sun, S., Sun, Y., and Liu, Z. (2022). Development and transdifferentiation into inner hair cells require Tbx2. Natl Sci Rev *9*, nwac156. 10.1093/nsr/nwac156.

24. Garcia-Anoveros, J., Clancy, J.C., Foo, C.Z., Garcia-Gomez, I., Zhou, Y., Homma, K., Cheatham, M.A., and Duggan, A. (2022). Tbx2 is a master regulator of inner versus outer hair cell differentiation. Nature *605*, 298-303. 10.1038/s41586-022-04668-3.

25. Kaiser, M., Ludtke, T.H., Deuper, L., Rudat, C., Christoffels, V.M., Kispert, A., and Trowe, M.O. (2022). TBX2 specifies and maintains inner hair and supporting cell fate in the Organ of Corti. Nat Commun *13*, 7628. 10.1038/s41467-022-35214-4.

26. Vahava, O., Morell, R., Lynch, E.D., Weiss, S., Kagan, M.E., Ahituv, N., Morrow, J.E., Lee, M.K., Skvorak, A.B., Morton, C.C., et al. (1998). Mutation in transcription factor POU4F3 associated with inherited progressive hearing loss in humans. Science *279*, 1950-1954. 10.1126/science.279.5358.1950.

27. Masuda, M., Dulon, D., Pak, K., Mullen, L.M., Li, Y., Erkman, L., and Ryan, A.F. (2011). Regulation of POU4F3 gene expression in hair cells by 5' DNA in mice. Neuroscience *197*, 48-64.

10.1016/j.neuroscience.2011.09.033.

28. Xiang, M., Gan, L., Li, D., Chen, Z.Y., Zhou, L., O'Malley, B.W., Jr., Klein, W., and Nathans, J. (1997). Essential role of POU-domain factor Brn-3c in auditory and vestibular hair cell development. Proc Natl Acad Sci U S A *94*, 9445-9450. 10.1073/pnas.94.17.9445.

29. Zhu, G.J., Gong, S., Ma, D.B., Tao, T., He, W.Q., Zhang, L., Wang, F., Qian, X.Y., Zhou, H., Fan, C., et al. (2020). Aldh inhibitor restores auditory function in a mouse model of human deafness. PLoS Genet *16*, e1009040. 10.1371/journal.pgen.1009040.

30. Erkman, L., McEvilly, R.J., Luo, L., Ryan, A.K., Hooshmand, F., O'Connell, S.M., Keithley, E.M., Rapaport, D.H., Ryan, A.F., and Rosenfeld, M.G. (1996). Role of transcription factors Brn-3.1 and Brn-3.2 in auditory and visual system development. Nature *381*, 603-606. 10.1038/381603a0.

31. Xiang, M., Gao, W.Q., Hasson, T., and Shin, J.J. (1998). Requirement for Brn-3c in maturation and survival, but not in fate determination of inner ear hair cells. Development *125*, 3935-3946. 10.1242/dev.125.20.3935.

32. Yu, H.V., Tao, L., Llamas, J., Wang, X., Nguyen, J.D., Trecek, T., and Segil, N. (2021). POU4F3 pioneer activity enables ATOH1 to drive diverse mechanoreceptor differentiation through a feed-forward epigenetic mechanism. Proc Natl Acad Sci U S A *118*. 10.1073/pnas.2105137118.

33. Wallis, D., Hamblen, M., Zhou, Y., Venken, K.J., Schumacher, A., Grimes, H.L., Zoghbi, H.Y., Orkin, S.H., and Bellen, H.J. (2003). The zinc finger transcription factor Gfi1, implicated in lymphomagenesis, is required for inner ear hair cell differentiation and survival. Development *130*, 221-232. 10.1242/dev.00190.

34. Hertzano, R., Montcouquiol, M., Rashi-Elkeles, S., Elkon, R., Yucel, R., Frankel, W.N., Rechavi, G., Moroy, T., Friedman, T.B., Kelley, M.W., and Avraham, K.B. (2004). Transcription profiling of inner ears from Pou4f3(ddl/ddl) identifies Gfi1 as a target of the Pou4f3 deafness gene. Hum Mol Genet *13*, 2143-2153. 10.1093/hmg/ddh218.

35. Grifone, R., Saquet, A., Xu, Z., and Shi, D.L. (2018). Expression patterns of Rbm24 in lens, nasal epithelium, and inner ear during mouse embryonic development. Dev Dyn *247*, 1160-1169. 10.1002/dvdy.24666.

36. Wang, G., Li, C., He, S., and Liu, Z. (2021). Mosaic CRISPR-stop enables rapid phenotyping of nonsense mutations in essential genes. Development. 10.1242/dev.196899.

37. Zhang, H., Pan, H., Zhou, C., Wei, Y., Ying, W., Li, S., Wang, G., Li, C., Ren, Y., Li, G., et al. (2018). Simultaneous zygotic inactivation of multiple genes in mouse through CRISPR/Cas9-mediated base editing. Development *145*. 10.1242/dev.168906.

38. Matern, M., Vijayakumar, S., Margulies, Z., Milon, B., Song, Y., Elkon, R., Zhang, X., Jones, S.M., and Hertzano, R. (2017). Gfi1(Cre) mice have early onset progressive hearing loss and induce recombination in numerous inner ear non-hair cells. Sci Rep *7*, 42079. 10.1038/srep42079.

39. Yang, H., Gan, J., Xie, X., Deng, M., Feng, L., Chen, X., Gao, Z., and Gan, L. (2010). Gfi1-Cre knock-in mouse line: A tool for inner ear hair cell-specific gene deletion. Genesis *48*, 400-406. 10.1002/dvg.20632.

40. Matern, M.S., Milon, B., Lipford, E.L., McMurray, M., Ogawa, Y., Tkaczuk, A., Song, Y., Elkon, R., and Hertzano, R. (2020). GFI1 functions to repress neuronal gene expression in the developing inner ear hair cells. Development *147*. 10.1242/dev.186015.

41. Kothary, R., Clapoff, S., Darling, S., Perry, M.D., Moran, L.A., and Rossant, J. (1989). Inducible expression of an hsp68-lacZ hybrid gene in transgenic mice. Development *105*, 707-714.

42. Xu, J., Li, J., Zhang, T., Jiang, H., Ramakrishnan, A., Fritzsch, B., Shen, L., and Xu, P.X. (2021). Chromatin remodelers and lineage-specific factors interact to target enhancers to establish proneurosensory fate within otic ectoderm. Proc Natl Acad Sci U S A *118*. 10.1073/pnas.2025196118.

43. Shu, M., Hong, D., Lin, H., Zhang, J., Luo, Z., Du, Y., Sun, Z., Yin, M., Yin, Y., Liu, L., et al. (2022). Single-cell chromatin accessibility identifies enhancer networks driving gene expression during spinal cord development in mouse. Dev Cell *57*, 2761-2775 e2766. 10.1016/j.devcel.2022.11.011.

44. Sun, Y., Zhang, Y., Zhang, D., Wang, G., Song, L., and Liu, Z. (2022). In vivo CRISPR-Cas9-mediated DNA chop identifies a cochlear outer hair cell-specific enhancer. FASEB J *36*, e22233. 10.1096/fj.202100421RR.

45. Petit, C., Bonnet, C., and Safieddine, S. (2023). Deafness: from genetic architecture to gene therapy. Nat Rev Genet. 10.1038/s41576-023-00597-7.

46. Fritzsch, B., Matei, V.A., Nichols, D.H., Bermingham, N., Jones, K., Beisel, K.W., and Wang, V.Y. (2005). Atoh1 null mice show directed afferent fiber growth to undifferentiated ear sensory epithelia followed by incomplete fiber retention. Dev Dyn *233*, 570-583. 10.1002/dvdy.20370.

47. Atar, O., and Avraham, K.B. (2010). Anti-apoptotic factor z-Val-Ala-Asp-fluoromethylketone promotes the survival of cochlear hair cells in a mouse model for human deafness. Neuroscience *168*, 851-857. 10.1016/j.neuroscience.2010.04.011.

48. Liu, H., Giffen, K.P., Chen, L., Henderson, H.J., Cao, T.A., Kozeny, G.A., Beisel, K.W., Li, Y., and He, D.Z. (2022). Molecular and cytological profiling of biological aging of mouse cochlear inner and outer hair cells. Cell Rep *39*, 110665. 10.1016/j.celrep.2022.110665.

49. Sun, S., Li, S., Luo, Z., Ren, M., He, S., Wang, G., and Liu, Z. (2021). Dual expression of Atoh1 and Ikzf2 promotes transformation of adult cochlear supporting cells into outer hair cells. Elife *10*. 10.7554/eLife.66547.

50. Ranum, P.T., Goodwin, A.T., Yoshimura, H., Kolbe, D.L., Walls, W.D., Koh, J.Y., He, D.Z.Z., and Smith, R.J.H. (2019). Insights into the Biology of Hearing and Deafness Revealed by Single-Cell RNA Sequencing. Cell Rep *26*, 3160-3171 e3163. 10.1016/j.celrep.2019.02.053.

51. Wang, Y., Zhang, C., Peng, W., Du, H., Xi, Y., and Xu, Z. (2023). RBM24 is required for mouse

hair cell development through regulating pre-mRNA alternative splicing and mRNA stability. J Cell Physiol. 10.1002/jcp.31003.

52. Zheng, L., Yuan, H., Zhang, M., Wang, C., Cai, X., Liu, J., and Xu, X.Q. (2021). Rbm24 regulates inner-ear-specific alternative splicing and is essential for maintaining auditory and motor coordination. RNA Biol *18*, 468-480. 10.1080/15476286.2020.1817265.

53. Liu, L., Zou, L., Li, K., Hou, H., Hu, Q., Liu, S., Li, J., Song, C., Chen, J., Wang, S., et al. (2022). Template-independent genome editing in the Pcdh15(av-3j) mouse, a model of human DFNB23 nonsyndromic deafness. Cell Rep *40*, 111061. 10.1016/j.celrep.2022.111061.

54. Cai, T., Jen, H.I., Kang, H., Klisch, T.J., Zoghbi, H.Y., and Groves, A.K. (2015). Characterization of the transcriptome of nascent hair cells and identification of direct targets of the Atoh1 transcription factor. J Neurosci *35*, 5870-5883. 10.1523/JNEUROSCI.5083-14.2015.

55. Fiolka, K., Hertzano, R., Vassen, L., Zeng, H., Hermesh, O., Avraham, K.B., Duhrsen, U., and Moroy, T. (2006). Gfi1 and Gfi1b act equivalently in haematopoiesis, but have distinct, non-overlapping functions in inner ear development. EMBO Rep *7*, 326-333. 10.1038/sj.embor.7400618.

56. Tornari, C., Towers, E.R., Gale, J.E., and Dawson, S.J. (2014). Regulation of the orphan nuclear receptor Nr2f2 by the DFNA15 deafness gene Pou4f3. PLoS One *9*, e112247. 10.1371/journal.pone.0112247.

57. Towers, E.R., Kelly, J.J., Sud, R., Gale, J.E., and Dawson, S.J. (2011). Caprin-1 is a target of the deafness gene Pou4f3 and is recruited to stress granules in cochlear hair cells in response to ototoxic damage. J Cell Sci *124*, 1145-1155. 10.1242/jcs.076141.

58. Akil, O., Dyka, F., Calvet, C., Emptoz, A., Lahlou, G., Nouaille, S., Boutet de Monvel, J., Hardelin, J.P., Hauswirth, W.W., Avan, P., et al. (2019). Dual AAV-mediated gene therapy restores hearing in a DFNB9 mouse model. Proc Natl Acad Sci U S A *116*, 4496-4501. 10.1073/pnas.1817537116.

59. Tang, H., Wang, H., Wang, S., Hu, S.W., Lv, J., Xun, M., Gao, K., Wang, F., Chen, Y., Wang, D., et al. (2023). Hearing of Otof-deficient mice restored by trans-splicing of N- and C-terminal otoferlin. Hum Genet *142*, 289-304. 10.1007/s00439-022-02504-2.

60. Al-Moyed, H., Cepeda, A.P., Jung, S., Moser, T., Kugler, S., and Reisinger, E. (2019). A dual-AAV approach restores fast exocytosis and partially rescues auditory function in deaf otoferlin knock-out mice. EMBO Mol Med *11*. 10.15252/emmm.201809396.

61. Akil, O., Seal, R.P., Burke, K., Wang, C., Alemi, A., During, M., Edwards, R.H., and Lustig, L.R. (2012). Restoration of hearing in the VGLUT3 knockout mouse using virally mediated gene therapy. Neuron *75*, 283-293. 10.1016/j.neuron.2012.05.019.

62. Tan, F., Chu, C., Qi, J., Li, W., You, D., Li, K., Chen, X., Zhao, W., Cheng, C., Liu, X., et al. (2019). AAV-ie enables safe and efficient gene transfer to inner ear cells. Nat Commun *10*, 3733. 10.1038/s41467-019-11687-8.

63. Wu, J., Solanes, P., Nist-Lund, C., Spataro, S., Shubina-Oleinik, O., Marcovich, I., Goldberg, H., Schneider, B.L., and Holt, J.R. (2021). Single and Dual Vector Gene Therapy with AAV9-PHP.B Rescues Hearing in Tmc1 Mutant Mice. Mol Ther *29*, 973-988. 10.1016/j.ymthe.2020.11.016.

64. Isgrig, K., McDougald, D.S., Zhu, J., Wang, H.J., Bennett, J., and Chien, W.W. (2019). AAV2.7m8 is a powerful viral vector for inner ear gene therapy. Nat Commun *10*, 427. 10.1038/s41467-018-08243-1.

65. Landegger, L.D., Pan, B., Askew, C., Wassmer, S.J., Gluck, S.D., Galvin, A., Taylor, R., Forge, A., Stankovic, K.M., Holt, J.R., and Vandenberghe, L.H. (2017). A synthetic AAV vector enables safe and efficient gene transfer to the mammalian inner ear. Nat Biotechnol *35*, 280-284. 10.1038/nbt.3781.

66. Li, C., Shu, Y., Wang, G., Zhang, H., Lu, Y., Li, X., Li, G., Song, L., and Liu, Z. (2018). Characterizing a novel vGlut3-P2A-iCreER knockin mouse strain in cochlea. Hear Res *364*, 12-24. 10.1016/j.heares.2018.04.006.

67. Liu, Z., Owen, T., Zhang, L., and Zuo, J. (2010). Dynamic expression pattern of Sonic hedgehog in developing cochlear spiral ganglion neurons. Dev Dyn *239*, 1674-1683. 10.1002/dvdy.22302.

Figure Legends

Figure 1. Rbm24 expression is repressed in cochlear HCs in the absence of Pou4f3. (A) A simple illustration of how *Pou4f3* $^{-/-}$ strain was generated. **(B)** One exampled tail PCR gel image that helped us to distinguish WT (*Pou4f3*$^{+/+}$), heterozygous (*Pou4f3*$^{+/-}$) and homozygous (*Pou4f3*$^{-/-}$) mice. **(C-F'''**) Triple straining of Rbm24, Pou4f3 and Bcl11b in WT (C and E-E''') and *Pou4f3*$^{-/-}$ (D and F-F''') mice (n=3 for each) at E16.5, with only Rbm24 (green) channel was visualized in (C and D) at low magnification. (E-E''') and (F-F''') were the high magnification images of middle turn WT and *Pou4f3*$^{-/-}$ mice, respectively. In the absence of Pou4f3, Rbm24 expression completely disappeared, despite nascent Bcl11b+ OHCs were present. OHC: outer hair cell; IHC: inner hair cell. Scale bars: 100 µm (D), 20 µm (F''').

Figure 2. Gfi1 is dispensable for Rbm24 expression. (A) A simple cartoon representing how

the *Gfi1* was inactivated in the one-cell stage mouse zygotes derived from male *Gfi1*$^{HACre/+}$ by the CRISPR-stop approach. **(B-C)** With sgRNA-6 as an example, the Sanger sequencing chromatograms of control *Gfi1*$^{HACre/+}$ (B) and F0 *Gfi1*$^{-/-}$ (C) were presented. The base 'C' (black arrow in B) was converted in 'T' (red arrow in C), resulting in pre-emergence of protein translation stop codon TAG. The red 'T' was a single peak, meaning that the pre-emergence of stop codon occurred in both alleles. **(D-E")** Dual staining of HA (Gfi1) and Rbm24 in cochleae from control *Gfi1*$^{HACre/+}$ (D-D", n=3) and F0 *Gfi1*$^{-/-}$ (E-E") mice (n=4) at E16.5. Rbm24 expression (E') was not altered in the absence of the HA (Gfi1) expression (E). OHC: outer hair cell; IHC: inner hair cell. Scale bar: 20 μm.

Figure 3. Pou4f3 and Gfi1 expressions are normal in the absence of *Rbm24*. (A) A simple cartoon to elaborate how we used CRISPR-stop approach to induce mosaic inactivation of Rbm24 in the one-cell stage mouse zygote harboring *Gfi1*$^{HACre/+}$. Notably, the injection was in the late one-cell stage of the zygotes, resulting in higher rates of final mosaic inactivation. **(B-C)** The Sanger sequencing chromatograms of control *Gfi1*$^{HACre/+}$*; Rbm24*$^{+/+}$ (B) and *Gfi1*$^{HACre/+}$*; Rbm24*$^{-/-}$ (mosaic) (C). The base 'C' (black arrow in B) was converted into 'T' (red arrow in C) in a fraction of cochlear cells. Notably, the mosaic inactivation of Rbm24 was evidenced by the double peaks of 'T' and 'C' (red arrow in C). **(D-E"')** Triple staining of Rbm24, HA and Pou4f3 in cochlear samples (basal turns) of control *Gfi1*$^{HACre/+}$*; Rbm24*$^{+/+}$ (D-D"', n=3) and *Gfi1*$^{HACre/+}$*; Rbm24*$^{-/-}$ (mosaic) (E-E"', n=3) at E17. Consistent with the Sanger sequencing results (C), Rbm24 was inactivated in cochlear HCs in a mosaic pattern (E). The orange arrows (E-E"') pointed to one OHC that lost Rbm24, whereas the blue arrows (E-E"') marked one

OHC in which the Rbm24 expression was maintained. Notably, regardless of whether Rbm24 was inactivated or not, HA (Gfi1) and Pou4f3 expression were not altered. OHC: outer hair cell; IHC: inner hair cell. Scale bar: 20 μm (E''').

Figure 4. Three *Rbm24* enhancers are sufficient to drive specific EGFP expression in cochlear HCs. (A) Visualization of ATAC-seq (top row, orange color) of P1 cochlear HCs (from our previous study, GSE181311) and Pou4f3 Cut&Run assay (bottom row, blue color) of E17.5 cochlear HCs (from another study, GSE150391) by Integrative Genomics Viewer. The black arrow marked the *Rbm24* promoter, and the three *Rbm24* enhancers (Eh1, Eh2 and Eh3) were marked by the dotted square. **(B-G'')** Dual staining of EGFP and Myo7a in Eh1-EGFP+ (B-C'', n=7), Eh2-EGFP+ (D-E'', n=6) and Eh3-EGFP+ (F-G'', n=4) at P1. Only the EGFP channel was visualized in whole mount staining (B, D, F). In the cryosection cochlear samples, EGFP was overlapped with HC marker Myo7a. OHCs: outer hair cells; IHC: inner hair cell. Scale bars: 100 μm (F), 20 μm (G'').

Figure 5. Forced expression of Rbm24 fails to rescue the OHC degeneration in *Pou4f3*$^{-/-}$ mutants. (A) Generation of *Rosa26-Loxp-stop-Loxp-Rbm24*3×HA/+* (*Rosa26*$^{Rbm24/+}$) mouse stain. The C-terminus of the ectopic Rbm24 was tagged with three HA tags. **(B)** One exampled tail PCR gel image that helped us to distinguish WT (+/+) and KI (*Rosa26*$^{Rbm24/+}$) mice. **(C-F'')** Dual staining of HA (Rbm24) and hair cell marker Myo7a in mice with four different genotypes at P1: *Pou4f3*$^{+/+}$ (C-C'', n=3), *Pou4f3*$^{-/-}$ (D-D'', n=3) and *Pou4f3*$^{+/+}$; *Atoh1*$^{Cre/+}$; *Rosa26*$^{Rbm24/+}$ (E-E'', n=3) and *Pou4f3*$^{-/-}$; *Atoh1*$^{Cre/+}$; *Rosa26*$^{Rbm24/+}$ (F-F'', n=3). The ectopic HA (Rbm24) was

not detected in *Pou4f3*$^{+/+}$ (C) and *Pou4f3*$^{-/-}$ (D), but was detected in both *Pou4f3*$^{+/+}$; *Atoh1*$^{Cre/+}$; *Rosa26*$^{Rbm24/+}$ (E) and *Pou4f3*$^{-/-}$; *Atoh1*$^{Cre/+}$; *Rosa26*$^{Rbm24/+}$ (F). The white arrows in (E-E'') pointed to one Myo7a+ IHC that expressed the ectopic HA (Rbm24). The HCs seemed normal by P1, despite the ectopic Rbm24 expression was induced. The orange arrows in (E-E'') labelled one SC that expressed HA (Rbm24) but not Myo7a. The white arrows in (F-F'') should be one remaining Myo7a+ HC that expressed ectopic Rbm24. Overall, many of the *Pou4f3*$^{-/-}$ HCs degenerated, albeit ectopic Rbm24 was induced. OHC: outer hair cell; IHC: inner hair cell; HC: hair cell. Scale bar: 20 μm (F'').

Supplemental Figure Legends

Supplemental Figure 1. Rbm24 expression is repressed in cochlear HCs at E16.5 when Pou4f3 is inactivated. (A) An illustration of how *Pou4f3*$^{-/-}$ mice (Founder 0, F0) were rapidly generated by CRISPR-stop. **(B-C)** Sanger sequencing chromatograms of WT (B) and F0 *Pou4f3*$^{-/-}$ (C) were presented. The base 'C' (black arrow in B) was completely converted to 'T' (red arrow in C), resulting in pre-emergence of protein translation stop codon. The *Pou4f3*$^{-/-}$ mutants (F0 mice) were immediately ready for phenotypic analysis. **(D-E''')** Triple staining of pan-HC marker Pou4f3, Rbm24 and OHC marker Insm1 in whole mount prepared cochlear samples (basal turns) of WT (D-D''', n=3) and *Pou4f3*$^{-/-}$ (E-E''', n=9) at E16.5. Relative to WT mice, both Pou4f3 and Rbm24 expression disappeared in *Pou4f3*$^{-/-}$ HCs, whereas the Insm1 expression was normal. The orange arrows in (E-E''') pointed to one Insm1+ OHC that lost Pou4f3 and Rbm24. OHC: outer hair cell; IHC: inner hair cell. Scale bar: 20 μm (E''').

Supplemental Figure 2. Severe degeneration of *Pou4f3*$^{-/-}$ HCs happens by perinatal ages. (A-C") Dual staining of Pou4f3 and Myo7a in middle turn regions of the cochleae of WT (A-A") at P1 and *Pou4f3*$^{-/-}$ mice at P0 (B-B") and at P1 (C-C"). Notably, here the *Pou4f3*$^{-/-}$ mice were germ line stable strain produced by CRISPR/Cas9-mediated large DNA fragment deletion (Figure 1A). Arrows in (B-C") represented the surviving HCs in the absence of Pou4f3. **(D)** Quantification of the percentage of the remaining HCs at basal, middle, and apical turns in *Pou4f3*$^{-/-}$ mice at P0 (n=4) or at P1 (n=3), relative to WT mice at P1 (n=3). Data were presented as Mean ± Sem. Student's *t* test was used for statistical analysis. ** $p<0.01$; **** $p<0.0001$; n.s. no significant difference. HC degeneration at middle and basal turns was more severe at P1 than that at P0, but there was no significant difference in apical turns (D). **(E-F")** Dual staining of Rbm24 and Myo7a in WT (E-E", n=3) and *Pou4f3*$^{-/-}$ (F-F", n=3) mice at P1. The white arrow in (F-F") marked one remaining *Pou4f3*$^{-/-}$ HC that lost Rbm24 expression. OHC: outer hair cell; IHC: inner hair cell; HC: hair cell. Scale bar: 20 μm (C" and F").

Supplemental Figure 3. Construction of *Gfi1-3 ×HA-P2A-Cre/+* (*Gfi1*$^{HA\text{-}Cre/+}$) mouse model by which HA can faithfully represent Gfi1 expression. (A-C) A simple cartoon to illustrate how the *Gfi1*$^{HA\text{-}Cre/+}$ strain was constructed. Basically, the WT Gfi1 allele (A) was inserted a fragment containing 3 × HA-P2A-Cre (B) immediately before the TGA stop codon (red in A), resulting in a post-targeted *Gfi1*$^{HA\text{-}Cre/+}$ allele (C). **(D)** One exampled tail PCR gel image that helped us to distinguish *Gfi1*$^{+/+}$, *Gfi1*$^{HA\text{-}Cre/+}$ and *Gfi1*$^{HA\text{-}Cre/HA\text{-}Cre}$ mice. **(E-F")** Dual staining of HA (Gfi1) and HC marker Myo7a of control *Gfi1*$^{+/+}$ (E-E", n=3) and homozygous *Gfi1*$^{HA\text{-}Cre/HA\text{-}Cre}$ mice (F-F", n=3) at P1. Arrows in (F-F") marked one OHC that expressed HA (Gfi1)

and Myo7a. **(G-J")** Fate mapping analysis of cells experiencing *Gfi1* expression by *Gfi1*$^{HA\text{-}Cre/+}$; *Rosa26-loxp-stop-loxp-tdTomato* (Ai9)/+ (*Gfi1*$^{HA\text{-}Cre/+}$; Ai9/+), with confocal low magnification images being presented in (G-H"') and high magnification images in (I-J"). In Ai9/+ control mice at P2 (n=5), no Tdtomato+ cells were detected (G-G"' and I-I"). In contrast, in the *Gfi1*$^{HA\text{-}Cre/+}$; Ai9/+ mice (n=5), Tdtomato was detected in both non-sensory cells (white arrows in H) and the Myo7a+ HCs that expressed heterogeneous levels of HA (Gfi1), as represented in different arrows in (J-J"): white arrows (#1) marked one OHC with the highest HA (Gfi1), the orange arrows (#3) with the lowest (or undetectable) HA (Gfi1), and the blue arrows (#2) with the intermediate level of HA (Gfi1). Scale bars: 100μm in (H"'); 20 μm (F" and J").

Supplemental Figure 4. Gfi1 expression is lost in the *Pou4f3*$^{-/-}$ HCs. (A) One-step generation of *Pou4f3* mutants by CRISPR-stop, with the zygotes derived from the *Gfi1*$^{HA\text{-}Cre/+}$ mice. **(B-C)** Sanger sequencing chromatograms of tail DNA from the control *Gfi1*$^{HA\text{-}Cre/+}$ (B) and *Gfi1*$^{HA\text{-}Cre/+}$; *Pou4f3*$^{-/-}$ (mosaic) mice (C). The base 'C' in (blue arrow in B) was converted to 'T' (red arrow in C). However, the conversion was not complete because double peak existed, supporting that the inactivation of *Pou4f3* was mosaic. **(D-E"')** Triple staining of Pou4f3, Rbm24 and HA (Gfi1) in the basal region of cochleae of *Gfi1*$^{HA\text{-}Cre/+}$ (D-D"', n=3) and *Gfi1*$^{HA\text{-}Cre/+}$; *Pou4f3*$^{-/-}$ (mosaic, E-E"', n=3) at E16.5. Blue arrows in (E-E"') marked one OHC that expressed Pou4f3, Rbm24 and HA (Gfi1), whereas the orange arrows labelled the other OHC that lost Pou4f3, Rbm24 and HA (Gfi1). Thus, it confirmed that not only HA faithfully represented the Gfi1 expression, but also HA expression was dependent on Pou4f3. Scale bar:

20 μm (E''').

Supplemental Figure 5. Rbm24 expression is normal in the absence of *Gfi1*. (A) The DNA fragment between the sgRNA-4 and sgRNA-9 within the *Gfi1* locus was deleted by CRISPR/Cas9 method. **(B)** One exampled tail PCR gel image that helped us to distinguish *Gfi1*$^{+/+}$, *Gfi1*$^{+/-}$ and *Gfi1*$^{-/-}$ mice. **(C-D")** Dual staining of Pou4f3 and Rbm24 in middle turn cochleae of WT (C-C", n=3) and *Gfi1*$^{-/-}$ (D-D", n=3) at P1. Severe HC, especially OHC, degeneration happened in *Gfi1*$^{-/-}$ cochleae. The orange arrows in (D-D") marked one surviving *Gfi1*$^{-/-}$ OHC that expressed Pou4f3 and Rbm24. **(E-F''')** Triple staining of Pou4f3, Rbm24 and OHC marker Bcl11b of cochleae of WT (E-E''', n=3) and *Gfi1*$^{-/-}$ (F-F''', n=3) at E16.5. In terms of the expression patterns of Pou4f3, Rbm24 and Bcl11b, no significant difference was captured between WT and *Gfi1*$^{-/-}$ cochleae at E16.5, suggesting that *Gfi1*$^{-/-}$ HC degeneration did not start yet. Scale bars: 20 μm (D" and F''').

Figure 1

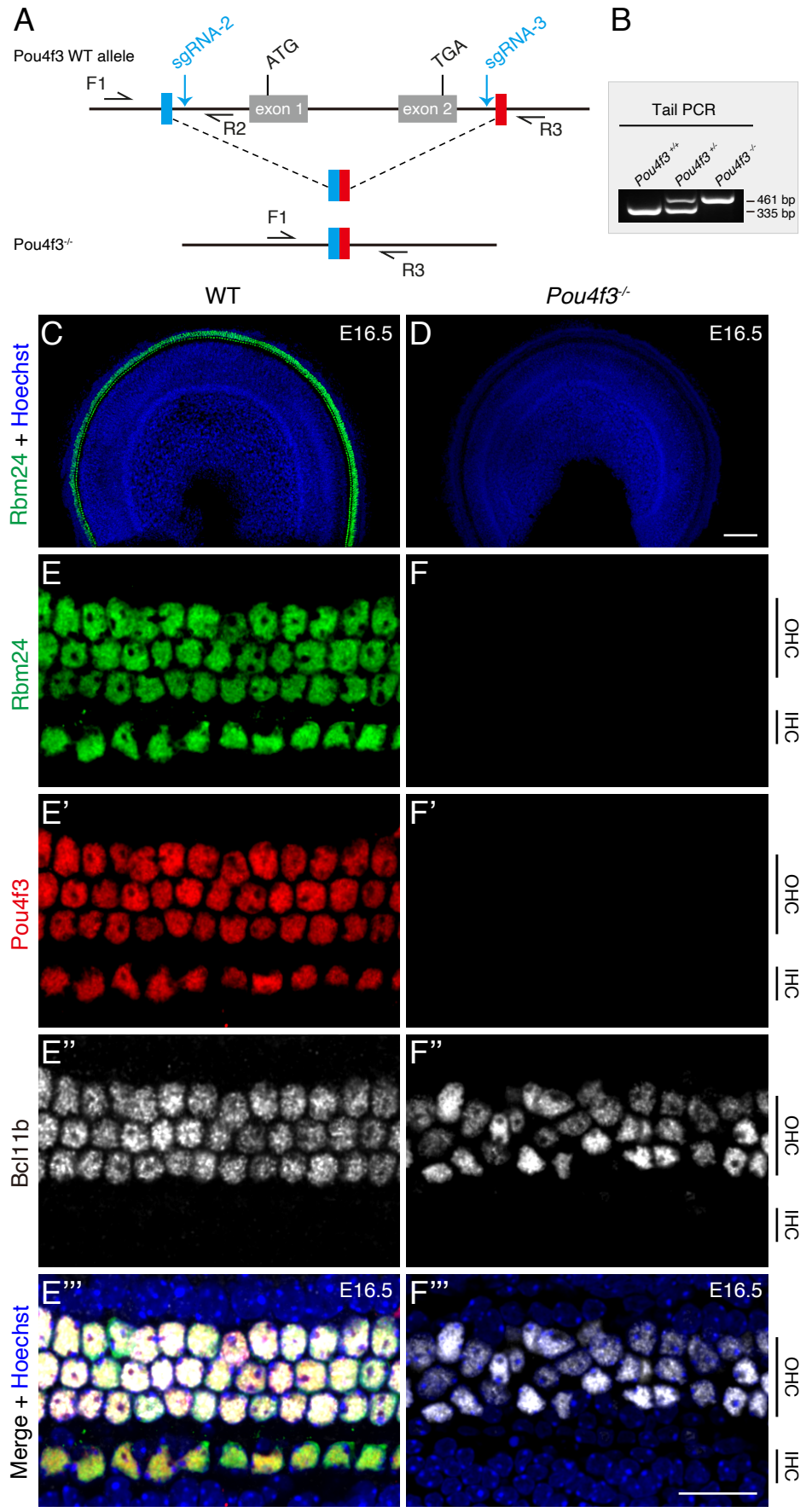
A
Pou4f3 WT allele
sgRNA-2
ATG
TGA
sgRNA-3
F1
exon 1
exon 2
R2
R3
F1
Pou4f3-/-
R3
B
Tail PCR
Pou4f3+/+
Pou4f3+/-
Pou4f3-/-
461 bp
335 bp
WT
Pou4f3-/-
C
E16.5
D
E16.5
Rbm24 + Hoechst
E
F
Rbm24
OHC
IHC
E'
F'
Pou4f3
OHC
IHC
E''
F''
Bcl11b
OHC
IHC
E'''
E16.5
F'''
E16.5
Merge + Hoechst
OHC
IHC

Figure 2

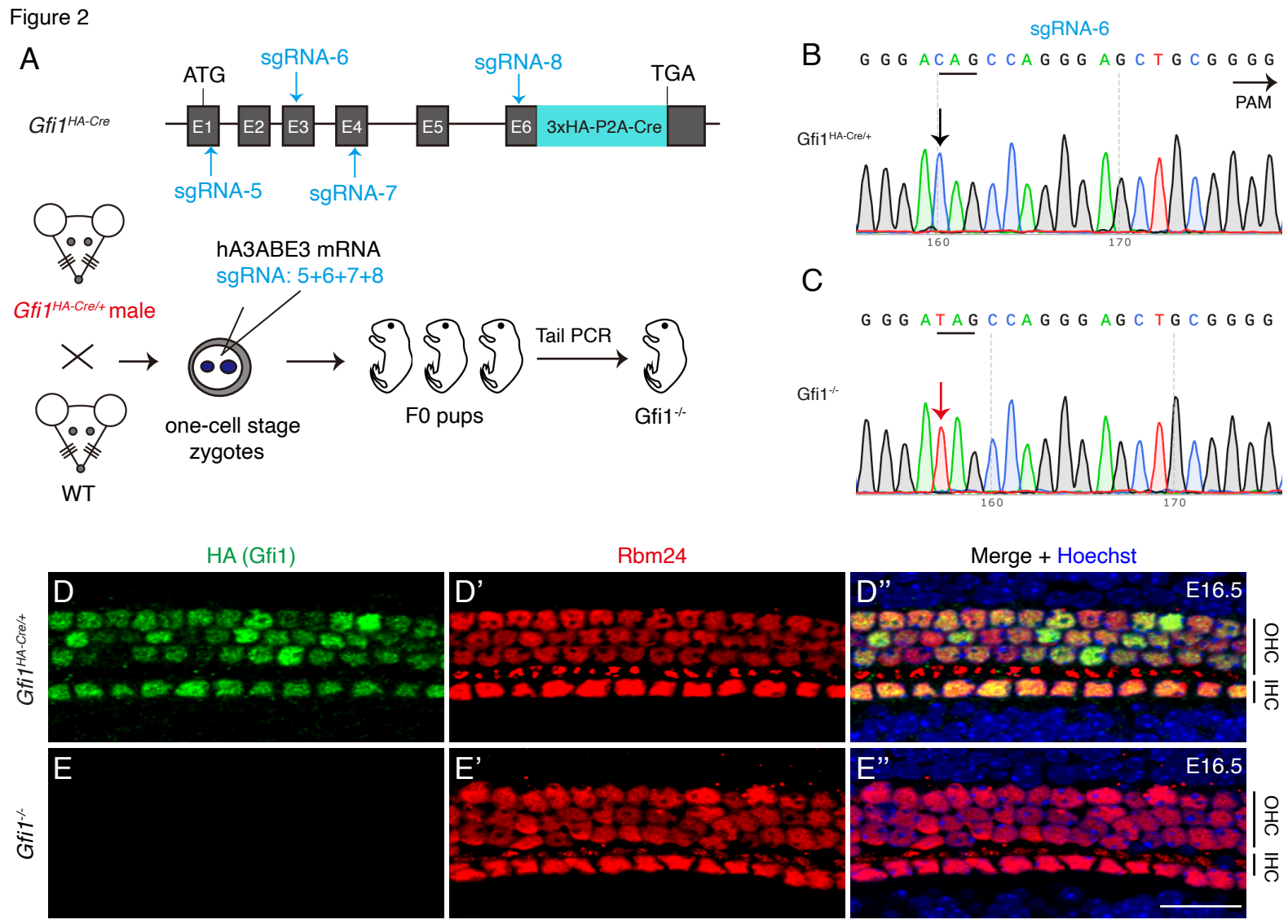
A
ATG
sgRNA-6
sgRNA-8
TGA
Gfi1HA-Cre
E1
E2
E3
E4
E5
E6
3xHA-P2A-Cre
sgRNA-5
sgRNA-7
hA3ABE3 mRNA
sgRNA: 5+6+7+8
Gfi1HA-Cre/+ male
WT
one-cell stage zygotes
F0 pups
Tail PCR
Gfi1-/-
B
sgRNA-6
G G G A C A G C C A G G G A G C T G C G G G G
PAM
Gfi1HA-Cre/+
160
170
C
G G G A T A G C C A G G G A G C T G C G G G G
Gfi1-/-
160
170
HA (Gfi1)
Rbm24
Merge + Hoechst
D
D'
D''
E16.5
OHC
IHC
Gfi1HA-Cre/+
E
E'
E''
E16.5
OHC
IHC
Gfi1-/-

Figure 3

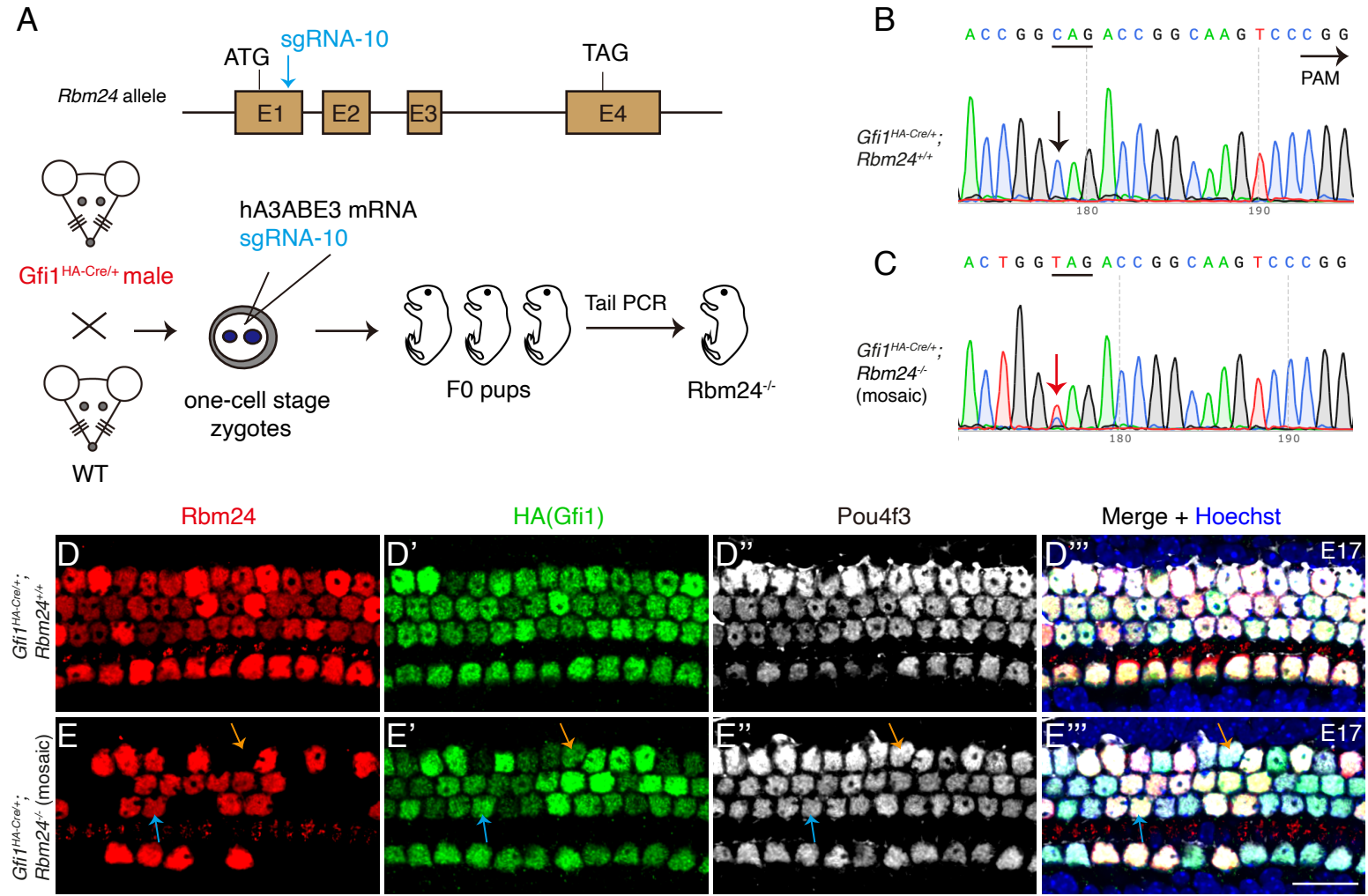
A
ATG
sgRNA-10
TAG
Rbm24 allele
E1
E2
E3
E4
Gfi1 HA-Cre/+ male
WT
hA3ABE3 mRNA
sgRNA-10
one-cell stage zygotes
F0 pups
Tail PCR
Rbm24-/-
B
A C C G G C A G A C C G G C A A G T C C C G G
PAM
Gfi1 HA-Cre/+; Rbm24+/+
180
190
C
A C T G G T A G A C C G G C A A G T C C C G G
Gfi1 HA-Cre/+; Rbm24-/- (mosaic)
180
190
Rbm24
HA(Gfi1)
Pou4f3
Merge + Hoechst
D
D'
D''
D'''
E17
OHC
IHC
Gfi1 HA-Cre/+; Rbm24+/+
E
E'
E''
E'''
E17
OHC
IHC
Gfi1 HA-Cre/+; Rbm24-/- (mosaic)

Figure 4

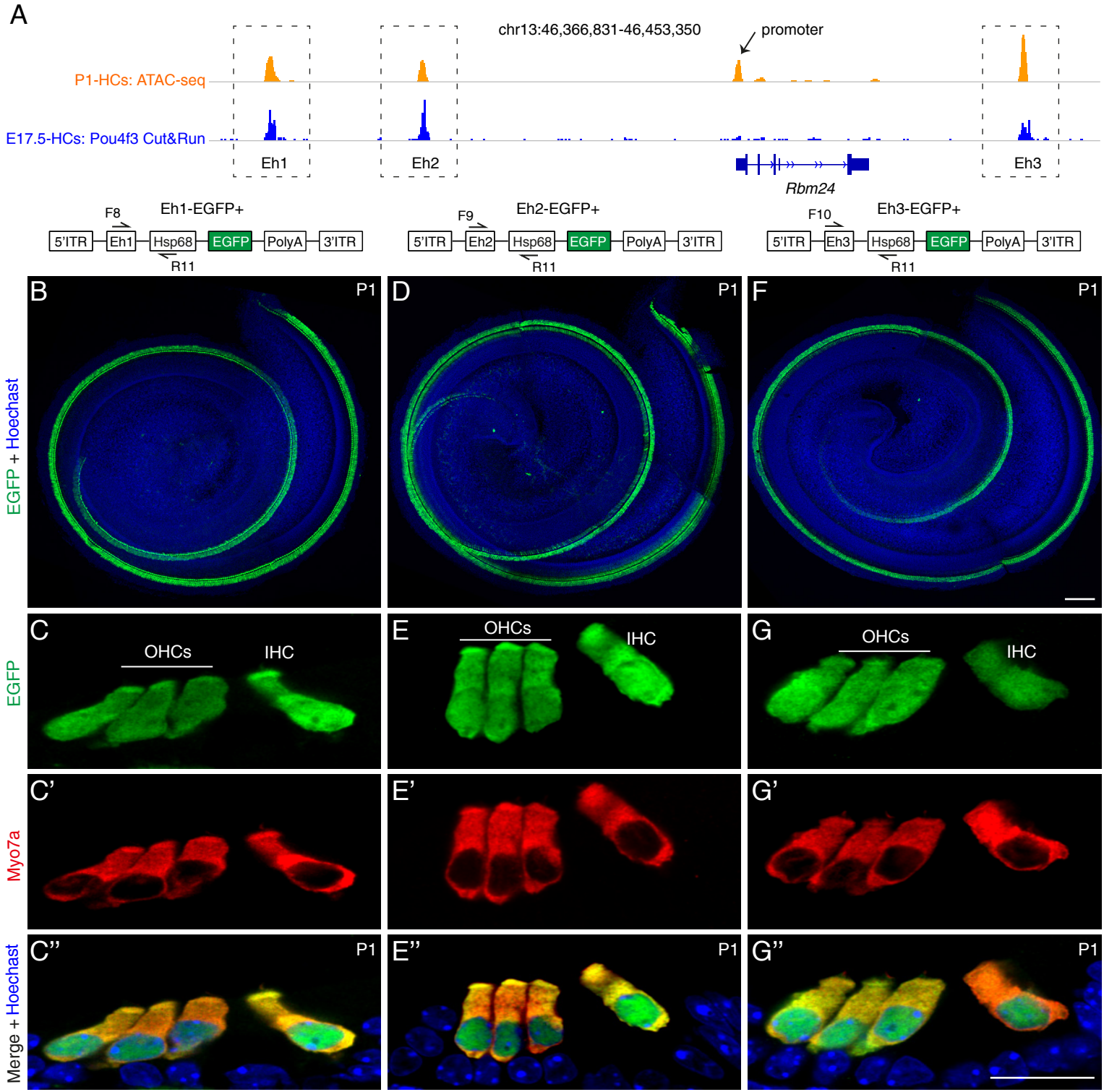
A
chr13:46,366,831-46,453,350
promoter
P1-HCs: ATAC-seq
E17.5-HCs: Pou4f3 Cut&Run
Eh1
Eh2
Eh3
Rbm24
F8
Eh1-EGFP+
5'ITR
Eh1
Hsp68
EGFP
PolyA
3'ITR
R11
F9
Eh2-EGFP+
Eh2
F10
Eh3-EGFP+
Eh3
B
D
F
P1
EGFP + Hoechast
C
E
G
OHCs
IHC
EGFP
C'
E'
G'
Myo7a
C''
E''
G''
Merge + Hoechast

Figure 5

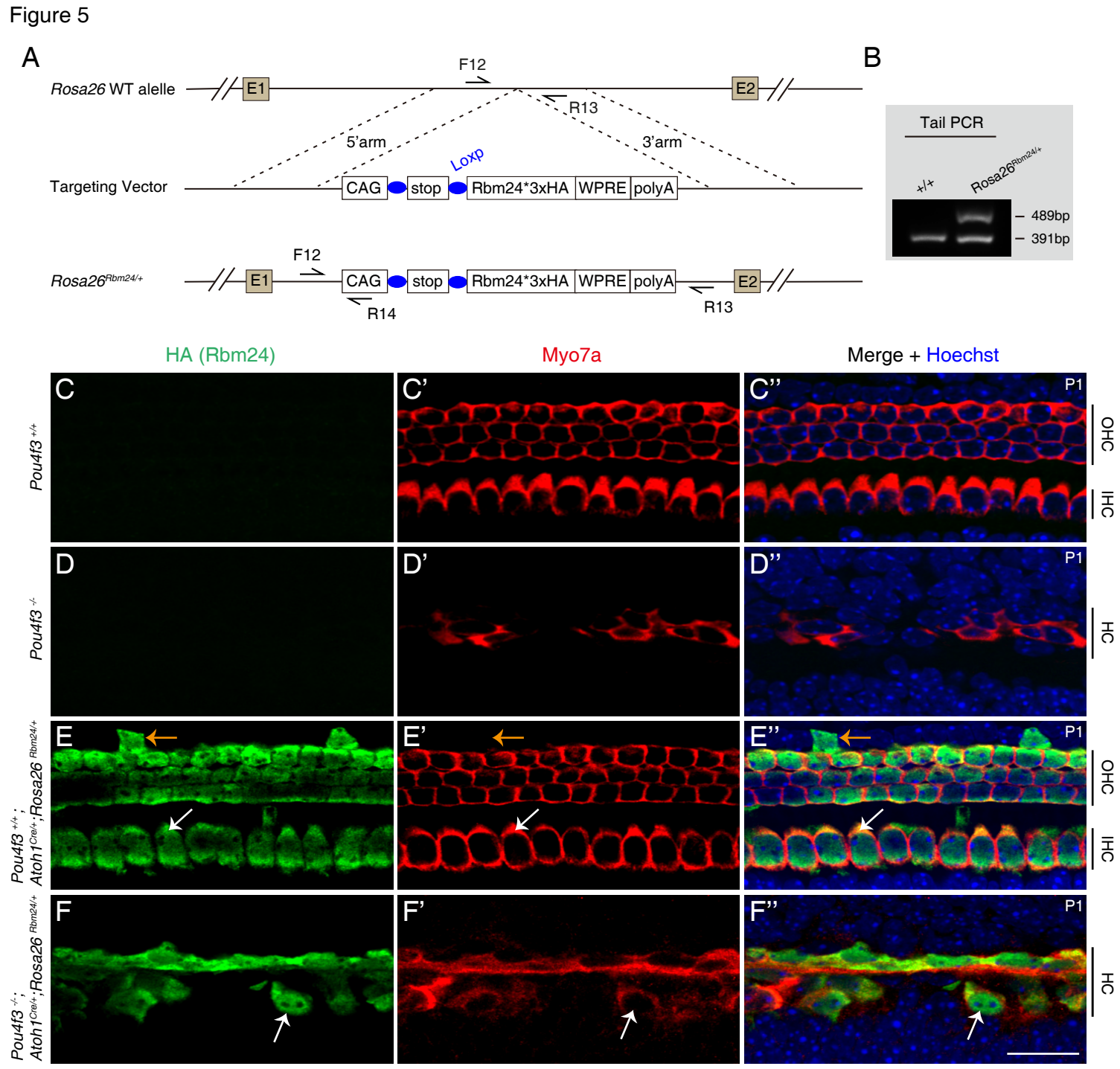
A
Rosa26 WT alelle
E1
E2
F12
R13
5'arm
3'arm
Loxp
Targeting Vector
CAG
stop
Rbm24*3xHA
WPRE
polyA
Rosa26Rbm24/+
F12
R14
R13
B
Tail PCR
+/+
Rosa26Rbm24/+
489bp
391bp
HA (Rbm24)
Myo7a
Merge + Hoechst
C
C'
C''
D
D'
D''
E
E'
E''
F
F'
F''
P1
OHC
IHC
HC
Pou4f3 +/+
Pou4f3 -/-
Pou4f3 +/+ ; Atoh1Cre/+;Rosa26 Rbm24/+
Pou4f3 -/- ; Atoh1Cre/+;Rosa26 Rbm24/+

Supplemental Figure 1

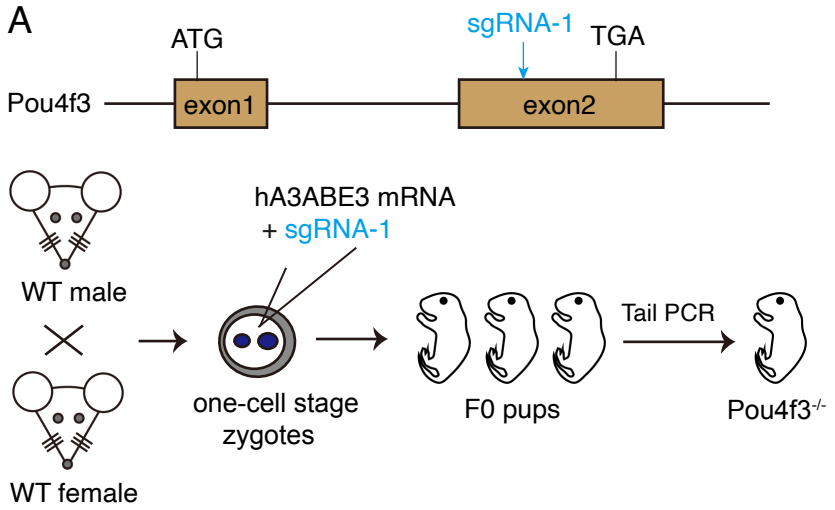

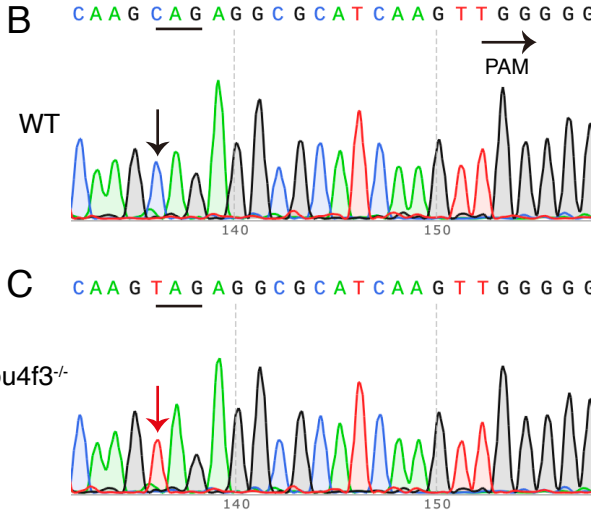

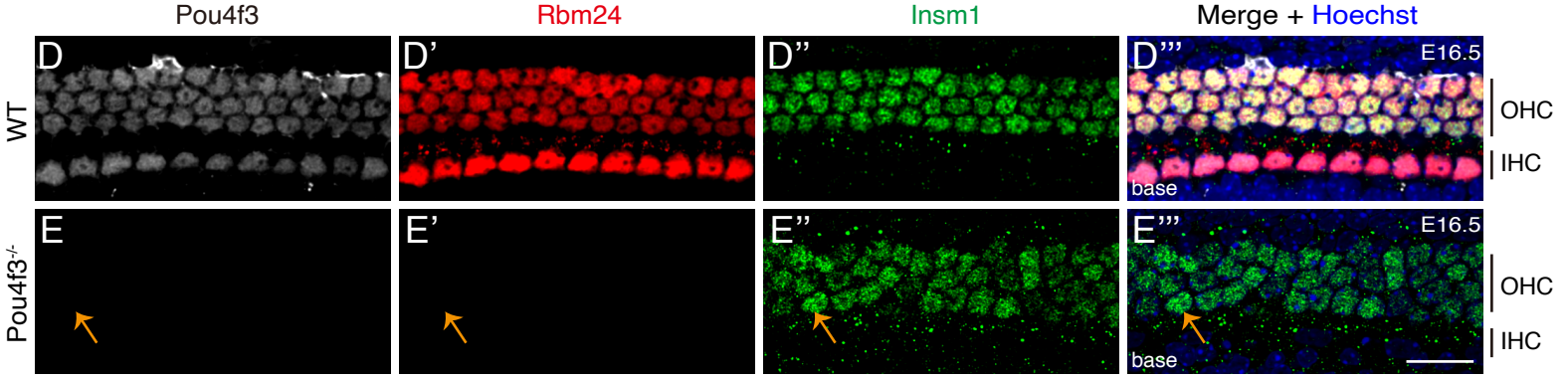

Supplemental Figure 2

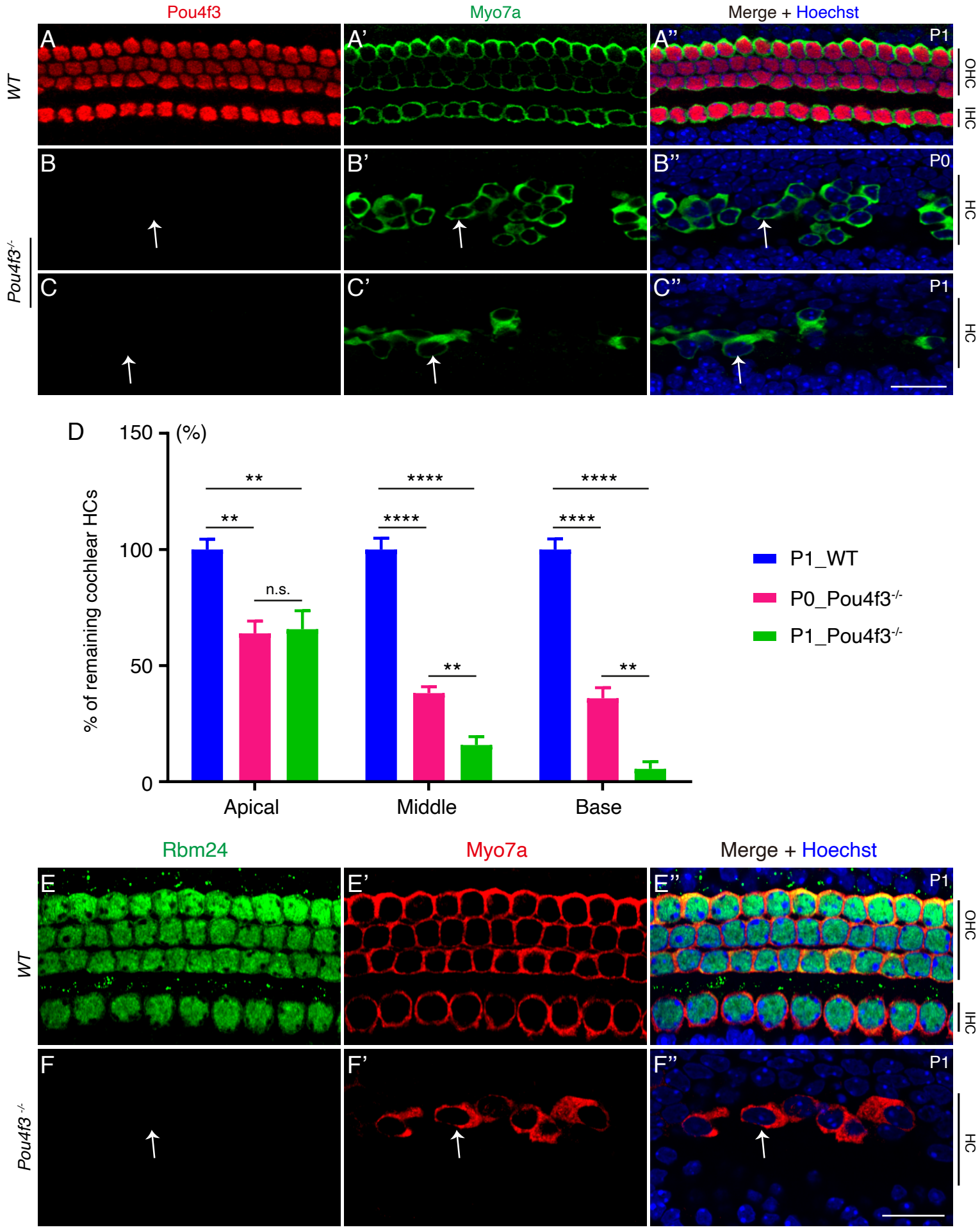

Supplemental Figure 3

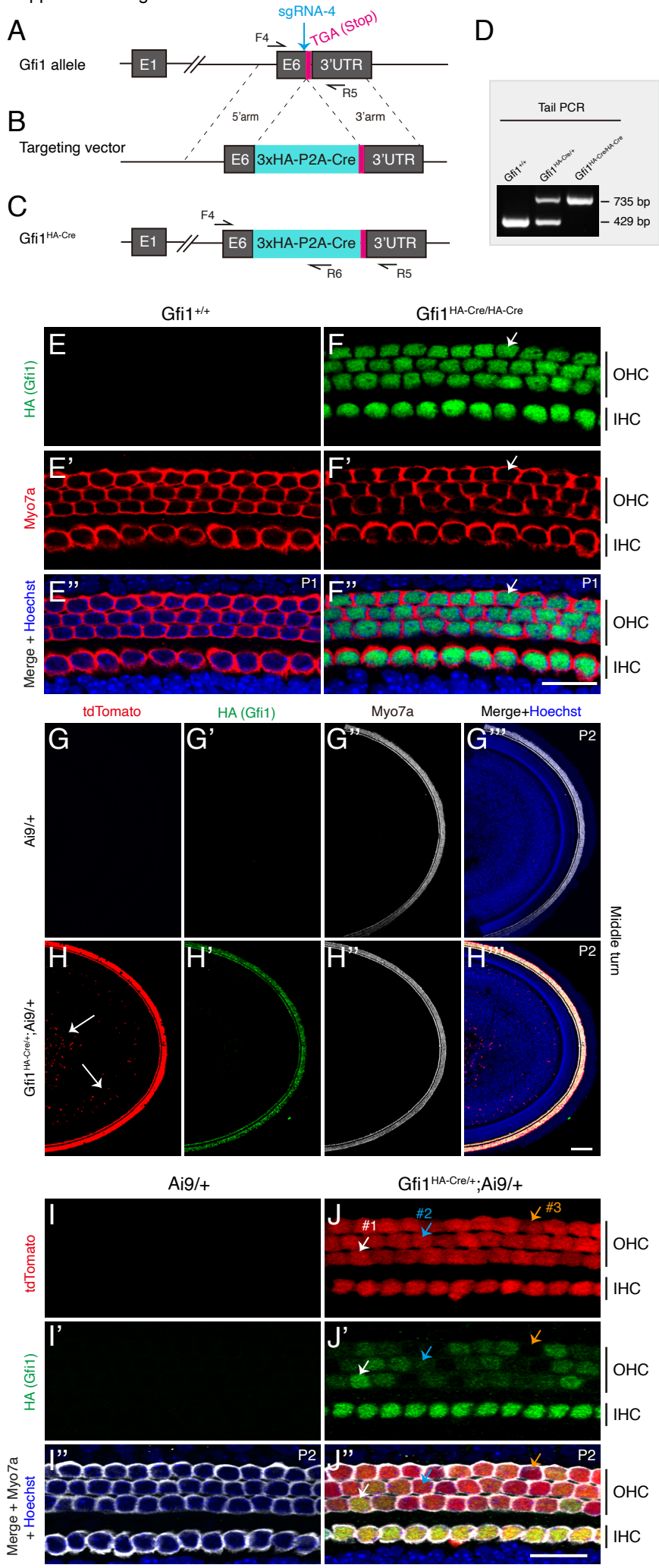

Supplemental Figure 4

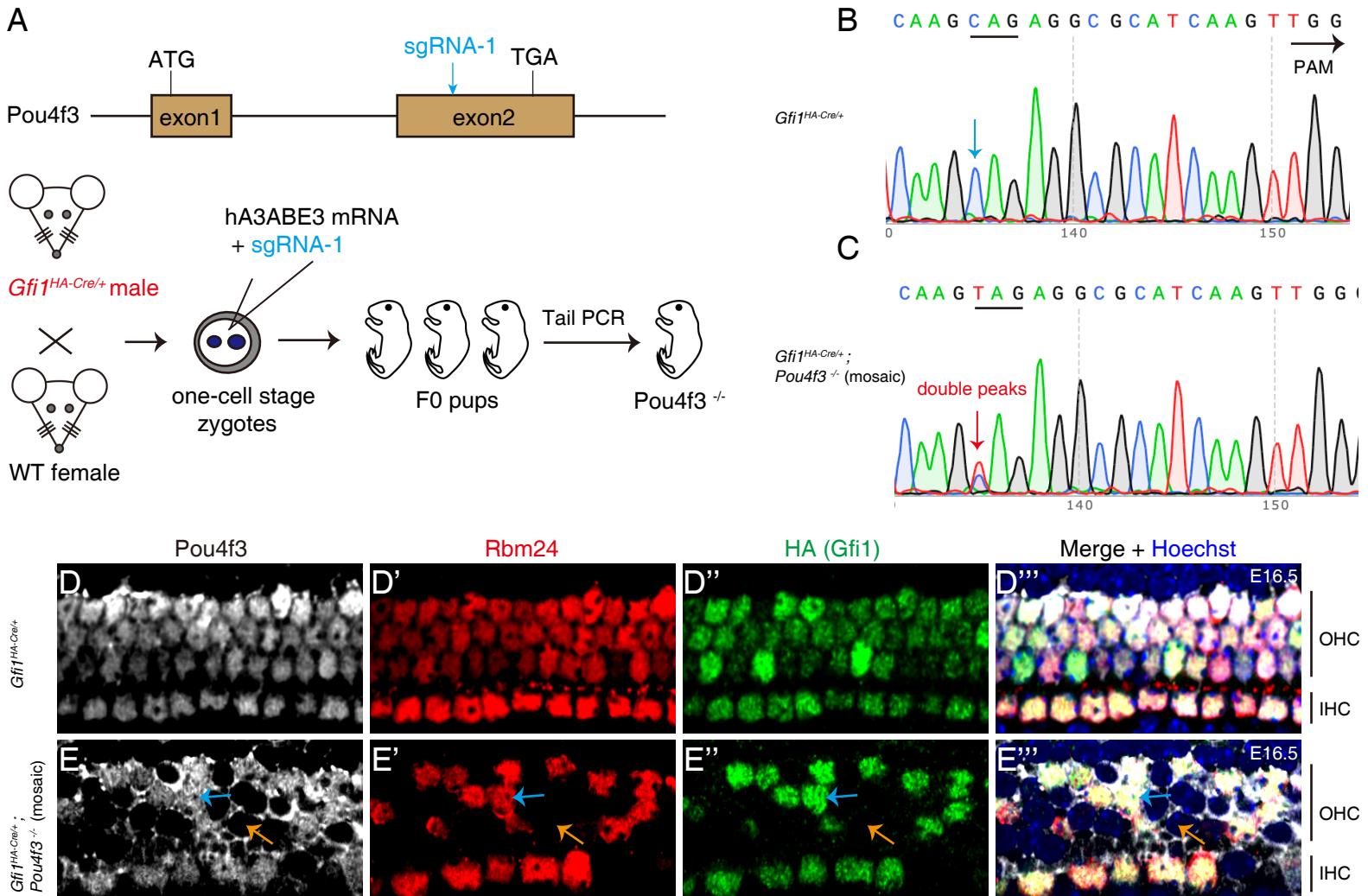
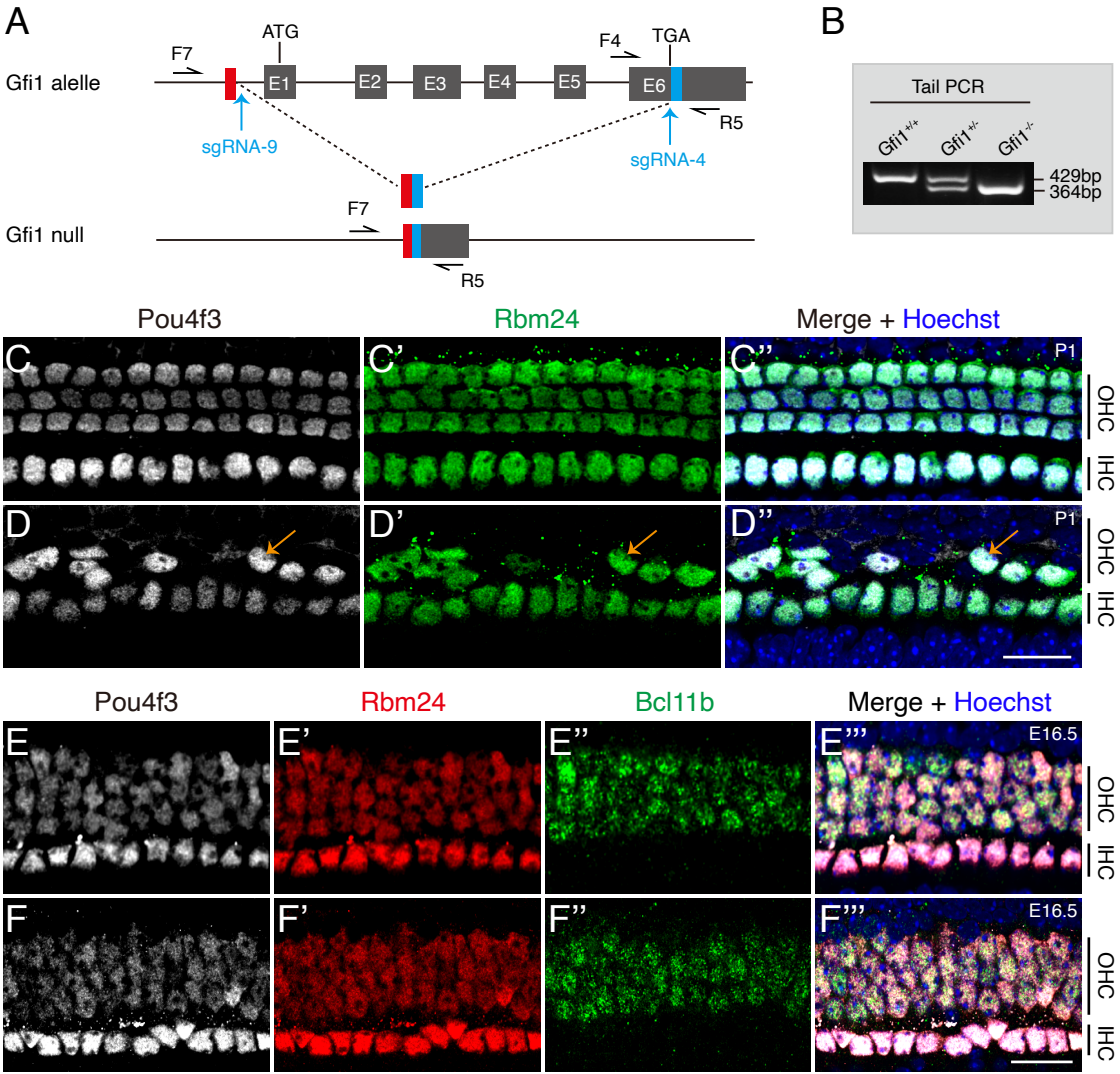
Supplemental Figure 5